# LANGMUIR

pubs.acs.org/Langmuir Article

## Simultaneous Electrophysiology and Imaging Reveal Changes in Lipid Membrane Thickness and Tension upon Uptake of Amphiphilic Gold Nanoparticles

Farzin Mashali, Colin M. Basham, Xufeng Xu, Camilla Servidio, Paulo H. Jacob Silva, Francesco Stellacci, and Stephen A. Sarles\*



Cite This: Langmuir 2023, 39, 15031-15045



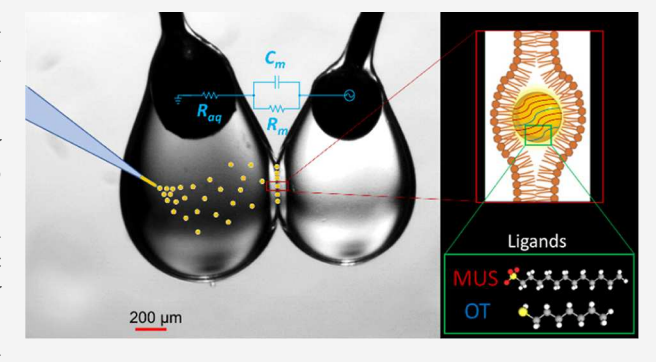
ACCESS I

III Metrics & More

Article Recommendations

Supporting Information

ABSTRACT: Amphiphilic gold core nanoparticles (AmNPs) striped with hydrophilic 11-mercapto-1-undecanesulfonate (MUS) and hydrophobic 1-octanethiol (OT) ligands are promising candidates for drug carriers that passively and nondisruptively enter cells. Yet, how they interact with cellular membranes is still only partially understood. Herein, we use electrophysiology and imaging to carefully assess changes in droplet interface bilayer lipid membranes (DIBs) incurred by striped AmNPs added via microinjection. We find that AmNPs spontaneously reduce the steady-state specific capacitance and contact angle of phosphatidylcholine DIBs by amounts dependent on the final NP concentration. These reductions, which are greater for NPs with a higher % OT ligands and



membranes containing unsaturated lipids but negligible for MUS-only-coated NPs, reveal that AmNPs passively embed in the interior of the bilayer where they increase membrane thickness and lateral tension through disruption of lipid packing. These results demonstrate the enhanced evaluation of nano-bio interactions possible via electrophysiology and imaging of DIBs.

#### INTRODUCTION

The growing interest in engineered nanomaterials for pharmaceutical, medical, cosmetic, and food applications increases concerns about their biocompatibility or toxicity and impact on human health. To help address these challenges, it is necessary to understand the fundamental events that occur at nano—bio interfaces, including biological membranes. Uncovering the mechanical and physiobiological effects of nanoparticles (NPs) on complex cellular membranes requires first gaining a thorough understanding of interactions between candidate engineered NPs and lipid bilayers. This knowledge is essential for designing and employing safe NPs for use as drug delivery agents, in diagnostics, and in other therapeutic applications.

One of the most frequently studied classes of NPs is surface-functionalized gold core NPs due to their highly tailorable surface properties. Gold NPs have been employed widely due to researchers' ability to tailor their surfaces using a variety of hydrophilic and hydrophobic functional groups that modulate their interactions with membranes. For example, citrate-capped gold NPs of varying sizes have shown to be wrapped by lipid bilayers via exchanging noncovalently bound citrate groups for direct lipid—gold interactions. Gold NPs with significant fractions of hydrophobic surface ligands, such as phospholipids or covalently bound alkanethiol monolayers, are known to irreversibly embed into the hydrophobic interior of a

bilayer or fully translocate across synthetic lipid membranes. These tendencies can be explained by the strong affinity of hydrophobic surface ligands on the NPs for the hydrophobic interior of the lipid membrane. The partitioning of NPs into a membrane and, thus, their resulting membrane activity and cytotoxicity are strongly determined by the hydrophobicity of NP surfaces. Consequently, incorporating fully hydrophobic NPs into biological environments can be problematic due to accumulation within and disruption of the membrane, along with agglomeration in aqueous media. 29,30

This understanding motivates retaining a substantial hydrophilic fraction of NP surface ligands,<sup>31</sup> which can result in an attractive balance of aqueous solubility and membrane affinity, and intentionally patterning the hydrophilic and hydrophobic ligands on the NP surface. In their seminal works, Stellacci et al. introduced spherical gold NPs coated with alternating striations of hydrophilic 11-mercapto-1-undecanesulfonate (MUS) and hydrophobic 1-octanethiol (OT) ligands.<sup>26,32–36</sup>

Received: July 14, 2023 Revised: September 20, 2023 Published: October 9, 2023





Due to their *stripy* surface patterns, these amphiphilic nanoparticles (AmNPs) were shown to passively reach the cytosols of living cells and carry molecular payloads through the outer plasma membranes, including via a nonendocytic and nondestructive transport pathway. <sup>26,33,37–39</sup> AmNPs were also stably soluble in aqueous media, allowing them to be readily delivered to living cells for a variety of potential therapeutic and diagnostic purposes.

Yet, stripy AmNPs have been experimentally studied only a few times using planar lipid membranes, 40-42 which offer advantages for controlling membrane composition and electrically interrogating particle-induced changes in the structural and transport properties of the bilayer. Possible NPmembrane interactions include adsorption onto or insertion into the bilayer, membrane translocation, lipid extraction, and pore formation, which could elicit changes in both the effective resistance and capacitance of a planar membrane. Carney et al. 42 first measured a spontaneous, NP concentration-dependent increase in nominal bilayer capacitance after introducing stripy AmNPs (ranging from 5 to 10 nm in diameter) to one side of a planar black lipid membrane (BLM). The equation for parallel plate capacitance,  $C = \varepsilon A/d$ , states that an increase in membrane permittivity  $(\varepsilon)$ , a growth in membrane area (A), or a decrease in dielectric thickness (d) could drive an increase in nominal capacitance. These authors concluded that particles smaller than 10 nm spontaneously embedded in the interior of the membrane as opposed to being surface-adsorbed.<sup>42</sup> Yet, they offered no explanations for why AmNPs caused nominal capacitance to rise instead of fall, they did not quantify changes in membrane conductance or area-normalized specific capacitance, and they did not investigate the possibility of particle translocation.4

Their results are also difficult to align with findings from other studies. For example, computer simulations by Van Lehn et al. 37,43 demonstrated that outward flipping—or snorkeling—of hydrophilic MUS ligands allows for hydrophobic interactions between OT ligands and lipid tails to be maximized in the center of the bilayer, enabling AmNPs to penetrate the bilayer midplane without greatly disrupting the bilayer but locally increasing its thickness. Thanges in transmembrane potential due to a difference in dipole or surface potentials of the two lipid leaflets can also skew values of nominal capacitance at a particular voltage. However, Carney et al. did not attempt to measure the transmembrane potential with particles present.

Additionally, researchers have measured the opposite change in the membrane capacitance upon exposure to other types of amphiphilic NPs. Guo et al.<sup>24</sup> reported a reduction in bilayer capacitance when planar bilayers were exposed to hydrophobic, lipid-covered NPs that embedded in, transiently porated, and then translocated across the membrane. Fleury et al.<sup>46</sup> also reported a reduction in bilayer capacitance and an increase in the ionic conductance of a DOPC planar bilayer upon interaction with surfactant-coated spiky gold NPs. Basham et al.<sup>47</sup> demonstrated that OT-coated hydrophobic gold NPs directly trapped in the center of the membrane increase bilayer thickness and reduce membrane capacitance. These contradictory accounts of the original measurements by Carney et al. highlight important gaps in our understanding of passive nanoscale interactions between stripy AmNPs and lipid membranes.

With this motivation in mind, we studied the effects of completely hydrophilic (MUS-only) and striped, amphiphilic

(MUS/OT) gold core NPs on the electrical properties of phosphatidylcholine planar lipid bilayers formed using the droplet interface bilayer (DIB) method. 48 We specifically hypothesized that (1) spontaneous absorption of MUS/OT AmNPs ( $\sim$ 5–6 nm total diameter) larger in diameter than the hydrophobic thickness of the bilayer (~3-4 nm) would increase the average thickness of the bilayer and thus reduce the specific capacitance of the membrane, without changing the inherent transmembrane potential and (2) sufficient association of particles with the membrane would affect other properties, including membrane conductance to ion transport and lateral membrane tension. To test these hypotheses, we used the DIB method rather than BLM because, in addition to allowing standard electrical interrogation, it enables directly controlling<sup>49</sup> and measuring<sup>50,51</sup> the area of the bilayer necessary for accurate estimates of membrane thickness. Imaging the connected droplet pair also allows for assessing the contact angle between droplets, a parameter that depends on lateral bilayer tension. 52 Thus, this combined capability makes for a more comprehensive experimental approach to study the physicochemical features of lipid bilayers and gain mechanistic insights into NP-bilayer interactions. 48,53

Nonetheless, the DIB approach also presents a challenge. While AmNPs are soluble in water,<sup>54</sup> we learned that adding them to the aqueous droplet solution prior to lipid monolayer assembly or bilayer formation in oil consistently leads to membrane rupture and droplet coalescence. This outcome motivated our previous work which revealed that stripy AmNPs and lipids exhibit synergistic assembly kinetics that likely lead to weakly bound NP-lipid complexes near or within the monolayer, increasing molecular disorder at the interface. 54 Thus, we employed microinjection through a pulled glass capillary to incorporate AmNPs directly into one or both droplets after either monolayer assembly or bilayer formation. Postbilayer injection has been leveraged by other groups to introduce proteins into DIB droplets \$55-57 and offers beforeand-after comparisons of bilayer properties. Injection of AmNPs after membrane assembly also approximates the manner in which therapeutically delivered NPs would interact with pre-existing biomembranes.

Therefore, we report on the use of direct microinjection of gold NPs into DIB droplets to study the changes in the membrane properties incurred by hydrophilic and stripy amphiphilic gold NPs. Area-normalized specific capacitance  $(C_{\rm m})$ , membrane resistance, and bilayer tension before and after NP injection were investigated by combining electrophysiological data with dual-view imaging. Notably, we found that  $C_{\rm m}$  reduces in a concentration-dependent manner after the addition of a critical concentration of AmNPs, incorporating particles on both sides of the membrane doubles the measured change in C<sub>m</sub>, and no significant change in transmembrane potential develops upon NP exposure. The steady-state reduction in C<sub>m</sub> and the minimum concentration required to cause a reduction is determined by the degree of hydrophobic functionalization of the AmNPs; hydrophilic NPs do not statistically change C<sub>m</sub>. AmNPs also cause a reduction in the droplet contact angle, which signifies an increase in bilayer tension and a decrease in bilayer adhesive energy. Collectively, these data suggest that above a certain concentration, stripy AmNPs in the aqueous phase spontaneously insert into the hydrophobic core of the planar bilayer, where they locally change the thickness of the membrane and laterally disrupt

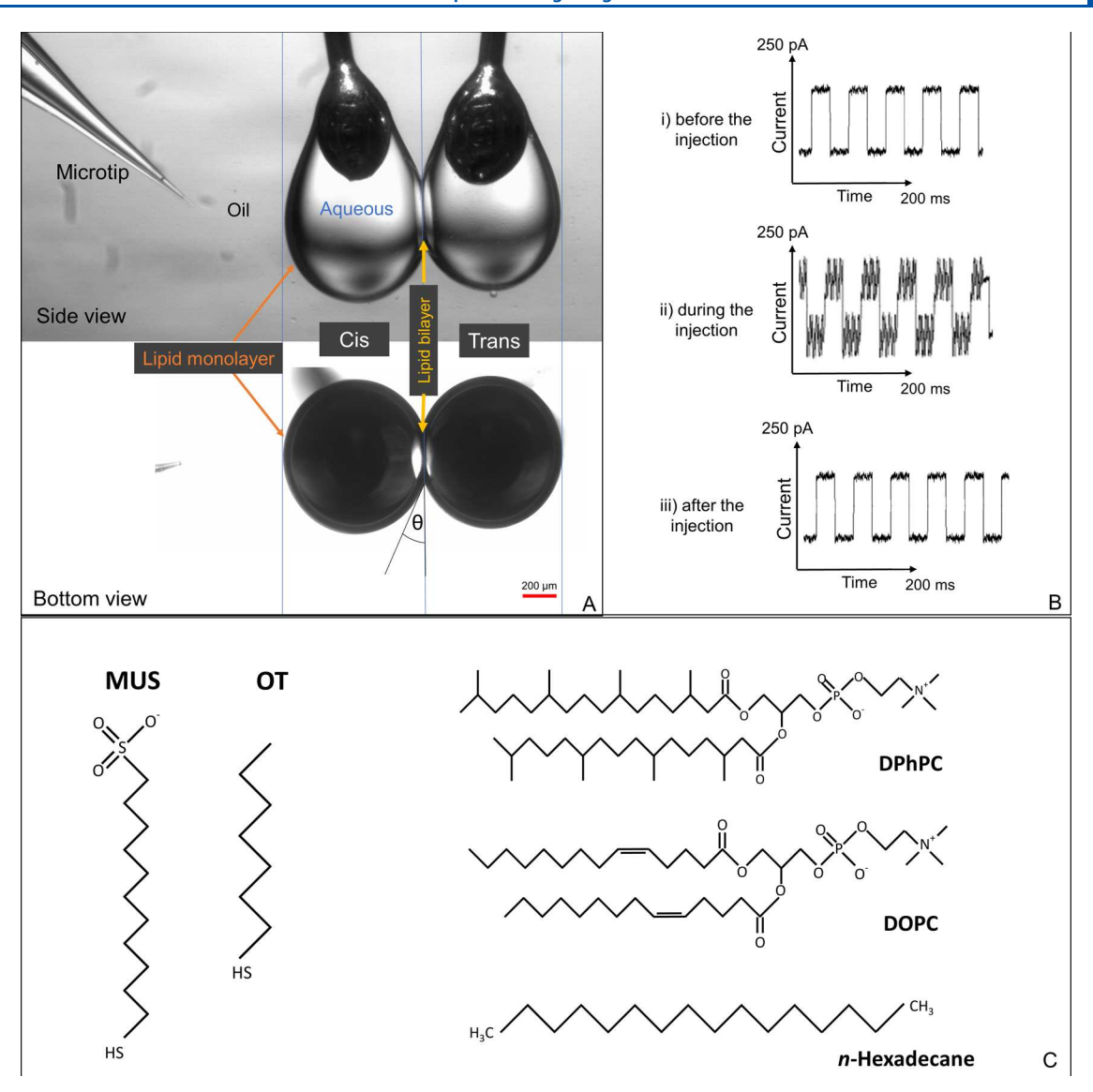


Figure 1. (A) Side and bottom view images provide accurate measurements of the bilayer area and droplet contact angle  $(\theta)$ . Arrows denote the projected lengths of the membrane in each view. (B) Rectangular capacitive current response to a triangular voltage input remains during NP injection, but a considerable amount of noise was observed when the pipet tip was inserted into the droplet. (C) Chemical structures of MUS and OT ligands on the NP's surface, DPhPC and DOPC lipids, and n-hexadecane oil used for DIB formation.

lipid packing. Furthermore, the experimental methods used demonstrate enhanced evaluation of nano-bio interactions.

#### RESULTS AND DISCUSSION

We specifically investigated the effects on lipid membranes caused by three types of surface-functionalized gold core NPs exhibiting varying amounts of hydrophobic surface ligands: those decorated solely with hydrophilic 11-mercapto-1-undecanesulfonate (MUS) ligands (henceforth, 0% OT NPs) and those decorated with both MUS and hydrophobic 1-octanethiol (OT) ligands at molar ratios of 85:15 MUS/OT (15% OT) and 70:30 MUS/OT (30% OT). Particle preparation and characterization are reported elsewhere.  $^{26,43,58,59}$  DLS measurements on these particles in 1× PBS find that their hydrated diameters are approximately 5–6 nm, demonstrating the additional size that the surface ligands add to the  $\sim\!\!3$  nm gold core observed in TEM imaging (Supporting Information Figure S1).

DIBs were assembled by using either diphytanoylphosphatidylcholine (DPhPC) lipids or a 1:1 molar ratio of DPhPC and dioleoylphosphatidylcholine (DOPC) lipids. The former is commonly used in DIB studies because the branched acyl chain structure of the lipid yields a stable, highly resistive bilayer membrane that has been well characterized. 51,60,61 The latter was selected because it also yields stable, highly resistant lipid bilayers and incorporates unsaturated DOPC lipids found in mammalian cells. We also hypothesized that the addition of DOPC lipids, which have a lower bending rigidity, 62 would increase the strength of interactions between NPs and the membrane due to greater conformational flexibility. DIBs were formed using either the lipid-in (i.e., liposomes added to the aqueous droplets) or lipid-out (i.e., lipids dissolved in the surrounding oil) approach; all DIBs were assembled in nhexadecane because it yields good bilayer stability and low residual oil in the membrane.<sup>52</sup> The chemical structures of the MUS and OT ligands are presented in Figure 1C along with structures for the lipids and oil used to assemble DIBs.

While the presence of stripy AmNPs in the droplet(s) prior to monolayer assembly leads to unstable bilayers, we found that a stable bilayer can still be successively formed and maintained if the NPs are injected either: (1) before bilayer formation, but after the lipid monolayer preassembles around the droplets, or (2) after bilayer formation between lipidcoated droplets. This study primarily used the latter approach; however, we observed in multiple experiments that addition of AmNPs into one droplet prior to bilayer formation delays the onset of bilayer thinning and slows the subsequent growth in membrane area during bilayer formation (see Supporting Information Note S1 and Figure S2). This result indicates that the presence of AmNPs near the monolayer impedes the conformational flexibility or lateral mobility of lipids involved in the formation of the interfacial bilayer, thereby establishing an energy barrier to the entropic removal of oil that enables the two opposing monolayers to come together. Similarly, we previously demonstrated that fully hydrophobic NPs coated only with OT ligands and dispersed in the oil phase can impede bilayer formation.<sup>47</sup>

Post-Bilayer Formation Microinjection of NPs. Because few studies to date have employed postbilayer formation injection into DIB droplets, we summarize the method here and discuss key observations. The experimental setup is schematically illustrated in Figure S2, and additional details of the procedure are described in Materials and Methods.

Incorporating NPs into droplets after bilayer formation requires gentle and accurate movements of the glass capillary and precise injection control to deliver nanoliter volumes. This approach enables before-and-after comparisons that are helpful to understand changes to the membrane caused by NPs injected near the bilayer. It also avoids the disruptive effects caused by coassembly of lipids and NPs at the oil-water interface that reduces DIB stability.<sup>54</sup> Therefore, we first formed a lipid bilayer between lipid-coated droplets on wiretype electrodes in oil via a standard protocol;<sup>52</sup> briefly, two aqueous droplets (150-300 nL) were incubated in oil until lipid monolayers self-assembled (~5 min), and then the droplets were maneuvered into contact. Bilayer formation was confirmed by an increase in contact area, as can be seen from below and from the side (Figure 1A) and the growth of squarewave capacitive current (Figure 1B) in response to a triangular AC voltage (10 Hz, 10 mV). The amplitude of the measured current signal was used to compute nominal membrane capacitance. After the membrane was formed, a micromanipulator was used to carefully insert the microtip of the pulled glass capillary (outer tip diameter:  $\sim 1.5 \mu m$ , as achieved by the protocol detailed in Materials and Methods), filled with aqueous NP solution, into the target droplet (cis droplet in Figure 1A). The capillary pressure was then raised pneumatically to establish outward flow of NP solution. The microinjection process took just a few seconds to deliver ~100 nL (see Video S1). Once the injected droplet reached an approximate desired volume, the microinjection pressure was reduced slightly, and the microtip was withdrawn from the droplet. Of note, when the microtip entered the droplet, the square, capacitive current waveform became noisy due to the electromagnetic interference introduced by the glass pipet (Figure 1B). This interference vanished when the microtip was removed from the droplet after controlled injection of NP solution, and it was further retracted from the proximity of the hanging droplets for subsequent electrical measurements.

The volume of injected NP solution was determined after each DIB experiment through image processing of the droplet dimensions obtained from bottom and side view images (Figure S4) before and after injection (Method described in Note S2). Based on the injected volumes ( $\sim 50-250$  nL), the estimated injection rate for a tip diameter of  $\sim 1.5~\mu m$  ranged from  $\sim 15$  to 25 nL/s. As long as the microtip was inserted slowly and the injection pressure was increased gradually, we found that the injection process did not reduce membrane stability nor immediately lead to noticeable increases in membrane conductance that might signify disruption to lipid packing.  $^{63}$ 

Still, the injection of an aqueous solution had noticeable effects on the connected droplet pair. Specifically, we observed that injecting aqueous solution into a lipid-coated droplet in oil immediately raised its interfacial tension, which caused it to adopt a more spherical shape and climb up the electrode (see Video S1). The injected droplet reverted to a pendant shape (Figure S5) within  $\sim$ 2–10 min upon adsorption of new lipids, which were present in excess within the droplet (or in the surrounding oil), reducing the interfacial tension at the oilwater interface back to a value near 1 mN/m. 64 These transient changes in the position of the injected droplet—along with the permanent increase in droplet volume—skewed the area of contact between droplets and reoriented the plane of the interfacial bilayer with respect to the two viewing perspectives. Thus, the positions of one or both droplets were manually adjusted via micromanipulators to reposition and reorient the planar bilayer such that it was located at the waistlines of the connected droplets and aligned in parallel to both the bottom view and side view cameras. These adjustments ensured accurate measurements of the bilayer lengths and apparent contact angles (measured only from the bottom view image, in a plane orthogonal to gravitational forces on the droplets; see Figure 1A) of the DIB, which were used to assess changes in the membrane area and tension.

AmNPs Cause Dose-Dependent Changes in Membrane Capacitance and DIB Contact Angle. Prior studies reported NP-induced changes in nominal membrane capacitance. Prior studies we hypothesized that membrane-active amphiphilic NPs would alter the value of DIB capacitance upon either the adsorption of NPs onto the membrane surface or penetration of NPs into the hydrophobic core of the bilayer. In particular, we chose to assess specific membrane capacitance,  $C_{\rm m}$  [ $\mu$ F/cm<sup>2</sup>] defined as

$$C_{\rm m} \equiv \frac{\Delta C}{\Delta A} = \frac{\varepsilon}{d} \tag{1}$$

because nominal membrane capacitance, C [F], alone can change due to alterations in area, A, thickness, d, or dielectric permittivity,  $\varepsilon$ . The DIB method allows for readily determining  $C_{\rm m}$  because the area of the bilayer can be carefully controlled and readily assessed from images. Examining  $C_{\rm m}$  rather than C is also critical since the contact area between droplets was mechanically manipulated upon repositioning the droplets after injection. Therefore, using methods reported in prior works, we measured  $C_{\rm m}$  on DIBs before and after injection of NPs. We found that changes in  $C_{\rm m}$  initiated a few minutes following injection of NPs and reached a steady state ~45 min after injection. In some cases, we also observed reductions in membrane resistance (Supporting Information; Note S3 and Figure S6), although this outcome was less

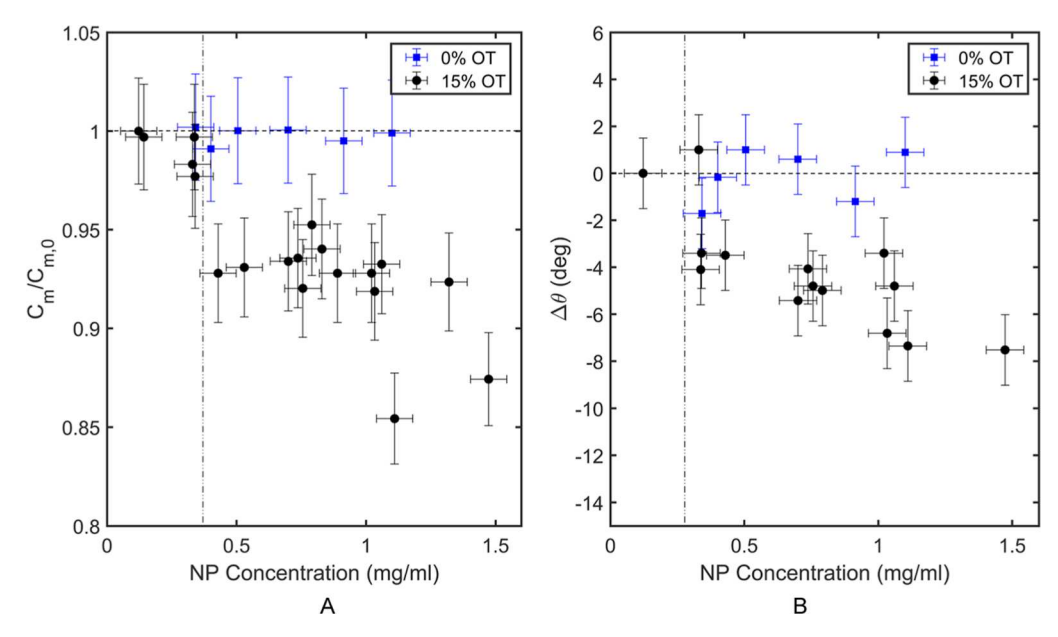


Figure 2. (A) Normalized specific capacitance  $(C_m/C_{m,0})$  of DPhPC bilayers versus final concentration of 0% OT and 15% OT NPs added to the cis droplet of a lipid-in DPhPC DIB. The vertical error bars represent the uncertainty in  $C_m$  ( $\pm 2.64\%$ ), and the horizontal error bars represent the uncertainty in concentration ( $\pm 0.07$  mg/mL). (B) Change in contact angle ( $\Delta \theta$ ) versus final concentration of 0% OT and 15% OT NPs added to the cis droplet of a lipid-in DPhPC DIB. The vertical error bars represent the uncertainty in  $\Delta \theta$  ( $\pm 1.5^{\circ}$ ), and the horizontal error bars represent the uncertainty in concentration ( $\pm 0.07$  mg/mL). In both plots, the horizontal dashed line indicates the normalized baseline measured in the absence of NPs, and the vertical dashed line marks the minimum concentration that causes a statistically significant change.

consistent. Therefore, we compare the steady-state changes in  $C_{\rm m}$  obtained 45–60 min after injection of NPs.

The average preinjection value of C<sub>m</sub> for a DPhPC bilayer formed in *n*-hexadecane was found to be  $C_{\rm m,0} = 0.65 \pm 0.02$  $\mu$ F/cm<sup>2</sup> (n = 8), consistent with reported values.<sup>52</sup> Injecting aqueous buffer without NPs into the cis droplet did not significantly change the specific capacitance ( $C_{\rm m} = 0.65 \pm 0.03$  $\mu F/cm^2$ , n = 5). Figure 2A shows the effects of varying concentrations of both 0% OT (100% MUS) and 15% OT (85% MUS) NPs added to the cis droplet on the normalized steady-state value of C<sub>m</sub> for DPhPC bilayers formed in nhexadecane. Each marker in this graph represents a separate DIB experiment (i.e., 19 in total for tests using 15% OT NPs) plotted versus the final NP concentration determined after injection of NP solution (see the Supporting Information; Note S2 and Figure S4). The vertical error bars shown for these data points represent the estimated uncertainty in the value of C<sub>m</sub>, stemming from limited accuracy in calculating bilayer area 50 due to difficulty in resolving the projected vertical length of the bilayer (ca. 200-400  $\mu$ m) captured by the side camera. Our conservative estimate of this measurement resolution is  $\pm 20 \ \mu m$  ( $\pm 5 \ pixels$ ), which leads to 1.5% uncertainty in the area and 2.64% uncertainty in C<sub>m</sub>. Higher image contrast in the bottom view images ensures better measurement of horizontal bilayer length. Therefore, we assume that the uncertainty in this imaging direction is negligible. The horizontal error bars represent uncertainty in the value of NP concentration ( $\pm 0.07$  mg/mL) due to approximations in assessing droplet volume after injection.

The data show that at sufficient concentrations, 15% OT NPs reduce the value of  $C_{\rm m}$  in a dose-dependent manner: higher NP concentrations lead to larger reductions in  $C_{\rm m}$ , as much as 18% below the average before-injection value,  $C_{\rm m,0}$ . Statistical comparisons described in the Materials and Methods section revealed the minimum threshold concentration to be

~0.4 mg/mL. A reduction in membrane capacitance caused by particle exposure is consistent with the findings of Guo et al., <sup>24</sup> who studied lipid-coated, dodecanethiol-functionalized gold NP, and Fleury et al., <sup>46</sup> who examined a surfactant-coated spiky gold NP. In sharp contrast, hydrophilic 0% OT NPs caused no significant changes to the value of specific capacitance for a DPhPC membrane at NP concentrations below or above 0.40 mg/mL. This finding is expected given the reduced (but not zero) energetic favorability of all MUS-coated NPs to insert into the membrane <sup>41,66</sup> and agrees with the insignificant changes in membrane capacitance reported by Carney et al. <sup>68</sup>

As described above, the cis droplet immediately moves up the electrode after injection of the NP solution due to the temporary increase in monolayer tension upon surface area expansion. This change also impacts the force balance that governs the equilibrium configuration of the interfacial bilayer. Specifically, the increase in monolayer tension at the droplet surface causes an abrupt decrease in the apparent contact angle between droplets. When the injected cis droplet droops again after the adsorption of new lipids, the contact angle rises but does not fully reach its initial value before injection for 15% OT NPs (time-dependent changes are shown in Figure S5). Accordingly, 15% OT NPs cause a dose-dependent reduction in the apparent steady-state contact angle that was not observed with 100% hydrophilic AuNPs (Figure 2B). For comparison, the dashed vertical line in this plot represents the same critical concentration determined from the  $C_m$  data (Figure 2A). In the absence of NPs, the apparent contact angle for DPhPC DIBs in *n*-hexadecane is  $\sim 30 \pm 1.5^{\circ}$ . Therefore, these reductions recorded for 15% OT NPs represent changes

Taken together, the data in Figure 2 reveal that 0% OT NPs (with only hydrophilic MUS ligands) do not alter either membrane capacitance or DIB contact angle at steady state,

whereas 15% OT NPs functionalized with both hydrophilic and hydrophobic ligands induce significant concentration-dependent changes to both parameters. These findings demonstrate that amphiphilic NPs are membrane active in a DPhPC DIB, whereas the gold NPs coated with only hydrophilic ligands are inert to the membrane.

Lipids in Oil and Higher OT Fractions Cause  $C_{\rm m}$  Reductions at Lower NP Doses. We further investigated the effect of NP hydrophobicity on changes in  $C_{\rm m}$  by comparing normalized values of steady-state  $C_{\rm m}$  after injecting 15 or 30% OT NPs into the *cis* droplet of DPhPC DIBs. While we were able to dissolve 0% OT and 15% OT NPs at concentrations up to 10 mg/mL in water, the maximum achievable concentration for 30% OT NPs was 0.16 mg/mL in water, determined via UV absorbance measurements (see Supporting Information; Note S4 and Figure S7). This constrained the range of concentrations of 30% OT NPs that could be exposed to the DIB.

Moreover, excess liposomes within the aqueous DIB droplets create a sink for sequestering membrane-active species away from the interfacial bilayer. Therefore, we compared the effects of 15% OT and 30% OT NPs using DPhPC DIBs formed by using the *lipid-out* approach. Relocating the lipids to the oil phase surrounding the droplets means that injected NPs are only able to interact with lipids at the droplet boundaries, and the only bilayer accessible to them is the one between the two droplets. Thus, a *lipid-out* approach better accomodated the lower solubility limit of 30% OT NPs in water and enabled us to investigate whether the detection limit for NP concentrations could be decreased for more sensitive electrophysiological analysis.

While the value of C<sub>m</sub> for DPhPC DIBs assembled using the lipid-in approach was not altered significantly at 15% OT NP concentrations below 0.40 mg/mL (Figure 2A), only 0.20 mg/ mL of the same NPs led to a significant reduction in  $C_m$  for DPhPC DIBs assembled from lipids-in-oil (Figure 3). The reductions in C<sub>m</sub> onset at considerably lower NP concentrations show that using a lipids-in-oil approach for DIB formation leads to a higher probability of the particles in the droplet interacting with the interfacial bilayer. The 30% OT NPs, which have a higher number of hydrophobic surface ligands, exhibited a stronger effect still: we observed a significant reduction in  $C_{\rm m}$  at a concentration of only 0.09 mg/mL (Figure 3), and the decrease in  $C_{\rm m}$  was larger (~8-10%) for 30% OT NPs than the ~3-5% decrease that occurred at higher concentrations of 15% OT NPs. These results demonstrate that increasing the percentage of hydrophobic ligands on the surface of the NP leads to a steeper reduction in  $C_{\rm m}$ , as well as lowers the minimum concentration required to reduce C<sub>m</sub>. This suggests a higher interaction strength between the membrane and 30% OT NPs compared to that incurred by 15% OT NPs.

AmNPs Cause Larger C<sub>m</sub> Reductions in Bilayers Containing DOPC Lipids. In addition to lipid placement and particle hydrophobicity, we examined the effect of membrane composition on the response of 15% OT amphiphilic NPs. Specifically, we formed DIBs using the *lipid-in* approach with either DPhPC or a 1:1 molar ratio of DPhPC and DOPC lipids supplied to the droplet as premixed liposomes. DOPC is commonly found in mammalian membranes and consists of unsaturated acyl chains that impart greater chain flexibility and reduce bending stiffness. <sup>69</sup> A 1:1 ratio of the two lipid types was chosen because it incorporates

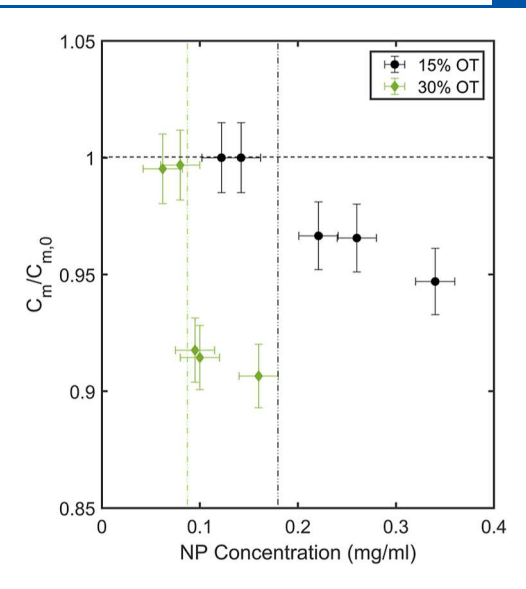


**Figure 3.** Normalized specific capacitance versus final NP concentration for 15% OT and 30% OT NPs tested using the *lipidout* configuration. The horizontal dashed line represents the normalized baseline concentration,  $C_{\rm m,0}/C_{\rm m,0}$  for a DPhPC bilayer in hexadecane. The vertical error bars represent the uncertainty in  $C_{\rm m}$  ( $\pm 2.64\%$ ), and horizontal error bars represent the uncertainty in concentration ( $\pm 0.02$  mg/mL). Green and black vertical dashed lines represent the minimum concentrations for  $C_{\rm m}$  reductions of 30% OT and 15% OT NPs, respectively.

a significant percentage of DOPC and still results in stable membranes with high membrane resistance. DIBs formed with only DOPC are inherently less stable and exhibit far lower values of membrane resistance, which lowers the sensitivity of electrophysiology measurements of membrane properties. <sup>47</sup> This was similarly observed in BLMs by Carney et al. <sup>70</sup>

Figure 4 shows the results of this comparison, where data for DPhPC membranes at similar final concentrations of injected NPs are compared to those obtained with DPhPC/DOPC DIBs. In the absence of NPs, DPhPC/DOPC bilayers exhibited an average  $C_{\rm m}$  value of 0.63  $\pm$  0.02  $\mu{\rm F/cm^2}$  (n = 5), very close to the value of  $C_{\rm m}$  for DPhPC bilayers. This suggests a nearly identical hydrophobic thickness for the two membrane compositions. 52 Similar to measurements on DPhPC membranes, reductions in  $C_{\rm m}$  were not observed for DPhPC/DOPC DIBs at NP concentrations below ~0.40 mg/ mL (Figure 4). However, above this threshold, the value of  $C_{\rm m}$ fell more sharply with an increasing NP concentration. Reductions of ~15% were obtained at concentrations between 0.70 and 1.0 mg/mL in the mixed lipid membranes. These data demonstrate that the strength of NP interactions also depends on the composition of the membrane. DOPC lipids exhibit a larger molecular area and a lower value of bending rigidity than DPhPC lipids. 47,71 These differences likely increase the amount of hydrophobic mismatch in the membrane interior and lower the energetic penalty to membrane bending, which favors the incorporation of spherical NPs to the hydrophobic core of the bilayer. Moreover, because we specifically varied the composition of the acyl chains and kept the phosphocholine headgroup the same, these data also suggest that particles interact with the hydrophobic acyl chains of the lipids in the membrane. This is discussed and quantified in a later section.

AmNPs in Both Droplets Cause Twice the Effect. We considered whether amphiphilic OT NPs adsorbed onto the outer surface of the bilayer were influencing the measured

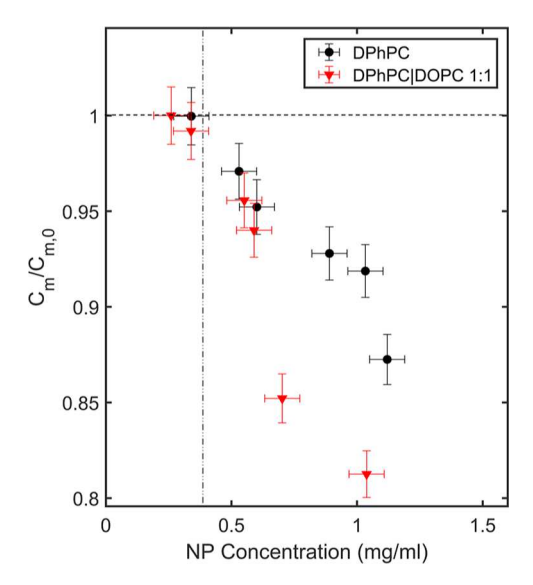


**Figure 4.** Comparing differences in  $C_{\rm m}/C_{\rm m,0}$  between bilayers formed with only DPhPC versus a 1:1 mixture of DOPC and DPhPC lipids after the addition of different concentrations of 15% OT NPs in a lipid-in configuration. It is shown that the reduction in  $C_{\rm m}$  is stronger in the DOPC/DPhPC mixture than in the DPhPC bilayer only. The horizontal dashed line indicates no changes in  $C_{\rm m}$  before and after injection. The vertical error bars represent the uncertainty in  $C_{\rm m}$  ( $\pm 2.64\%$ ), and the horizontal error bars represent the uncertainty in concentration ( $\pm 0.07~{\rm mg/mL}$ ).

changes in  $C_{\rm m}$ , especially since 0 and 15% OT NPs exhibit a net negative zeta potential (ca.  $-40~{\rm mV}$ ) in aqueous buffer. <sup>54</sup> Asymmetry in membrane lipid composition or adsorbed species establishes a transmembrane potential due to differences in surface or dipole potentials across the bilayer. A transmembrane potential alters the value of nominal capacitance measured at zero volts; its value can be determined by the voltage where capacitance is minimum. <sup>45</sup> Therefore, we

measured nominal bilayer capacitance versus voltage for a DIB in the presence and absence of 0 and 15% OT NPs to see if a transmembrane potential develops and whether this could explain the changes in C<sub>m</sub>. The results (see Figure S8) show that both 0 and 15% OT NPs added to the cis droplet (electrically grounded) shifts the location of minimum capacitance from 0 mV measured for no NPs to ca. -15 mV. This means that the cis droplet resides at a slightly lower potential than the trans droplet, likely from the association of adsorbed negatively charged NPs<sup>26</sup> on the cis leaflet of the membrane. This finding is consistent with our prior work examining interactions between MUS and MUS/OT NPs and lipid monolayers.<sup>54</sup> The fact that any nonzero transmembrane potential causes bilayer capacitance at 0 mV to be larger than its minimum value occurring in the absence of transmembrane potential means that shifts in transmembrane potential are not causing the reductions in C<sub>m</sub> reported when amphiphilic NPs are injected.

We were also curious about how adding particles to both sides of the membrane to re-establish symmetry would affect changes in specific capacitance. Therefore, we incorporated 15% OT NPs into both droplets of DIB through two separate microinjections: first into the cis droplet and then later into the trans droplet. Sufficient time between injections was allotted to assess the steady-state effect of each on  $C_{\rm m}$ , and similar final concentrations of NPs in each droplet were targeted to approximate symmetric NP loading. The values of  $C_m$  at these different stages for a representative experiment are shown in Figure 5. The key finding is that the injection of NPs into the trans droplet causes an additional decrease in the value of  $C_{\rm m}$ , not a reversal of the decrease evoked by the first injection. The first injection of NPs into the cis droplet lowered the value of  $C_{\rm m}$  by ~0.05  $\mu \rm F/cm^2$ , while the second injection reduced  $C_{\rm m}$ by another  $\sim 0.06 \, \mu \text{F/cm}^2$ . The blue star data point shows the final value of C<sub>m</sub> measured when 1.45 mg/mL of 15% OT NPs were injected only into the cis droplet of a separate DPhPC

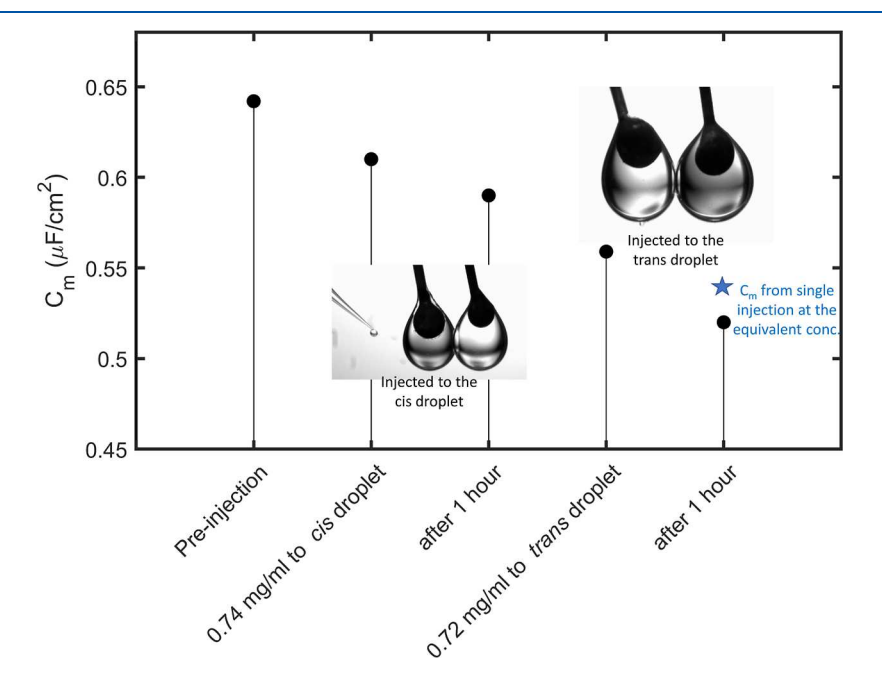


Figure 5. Specific capacitance of a DPhPC bilayer (filled circles) plotted across a multistep timeline in which 15% OT NPs are incorporated into first the *cis* droplet and then the *trans* droplet of a DIB. The blue star represents the steady-state value of  $C_{\rm m}$  for a separate DPhPC DIB in which 1.45 mg/mL was injected into only the *cis* droplet.

DIB. This comparison reveals that at a similar total number of particles incorporated into the system ( $\sim$ 0.70 mg/mL at 2× injected volume vs  $\sim$ 1.4 mg/mL at 1× volume), a larger reduction in  $C_{\rm m}$  occurs when particles are injected to both sides of the bilayer. This result differs from that of Carney et al., who reported no additional change upon the addition of particles into the *trans* reservoir. 70

This behavior was observed across multiple trials and suggests that changes in  $C_{\rm m}$  are due to particles embedding in the interior of the bilayer rather than only adsorbing to the surface and distorting the surface or dipole potentials of the lipid leaflet of the bilayer. The larger drop in  $C_{\rm m}$  upon symmetric loading at lower net concentrations indicates a greater ability for particles to incorporate into the membrane, a possibility due to fewer repulsive interactions between particles that might limit total incorporation or greater capacity of the lipids to rearrange around particles via insertion from two sides versus one.

AmNPs Increase Bilayer Thickness. The presented data reveal that amphiphilic NPs are membrane active, causing the specific capacitance of the membrane to be reduced in a concentration-dependent manner. A greater number of OT ligands on the particle surface lead to stronger reductions at lower NP concentrations in the aqueous solution adjacent to the bilayer. Bilayers containing unsaturated DOPC lipids exhibited larger reductions in  $C_{\rm m}$  compared to saturated DPhPC-only membranes at similar particle concentrations. Finally, injecting particles into both droplets instead of just one leads to greater reductions in  $C_{\rm m}$ , further proving that these changes do not stem from NP-induced alterations in the membrane surface potential or dipole potential. Instead, these measurements indicate that changes in specific capacitance are due to embedding of NPs into the inner hydrophobic region of the membrane, between lipid leaflets.

Equation 1 states that changes to either the dielectric permittivity or bilayer thickness can affect the value of  $C_m$ . One possibility is that NP insertion alters the effective dielectric permittivity of the hydrophobic membrane interior. The dielectric constant of gold is 6.9, while the permittivity of a hydrocarbon molecule is ~2.0-2.4. Thus, incorporation of gold core NPs would be expected to increase the effective dielectric constant of the membrane and, thereby, increase the value of the specific capacitance. Rather, we show convincingly that C<sub>m</sub> decreases upon NP exposure. Therefore, we conclude that particle interactions with the membrane which lower the value of  $C_{\rm m}$  must be the result of an increase in hydrophobic thickness of the membrane in addition to any changes in permittivity upon their incorporation. This rationale has been used previously to explain changes in nominal capacitance, but we cautiously approach the same conclusion here to avoid misinterpretation. 24,46,47

Quantifying the change in membrane thickness requires understanding how much the presence of surface-functionalized gold NPs in the membrane affects the dielectric constant of the membrane interior. It is known that the dielectric permittivity of aqueous or organic solutions of gold NPs is a frequency-dependent parameter: permittivity is maximum at low frequencies and decreases logarithmically with increasing frequency. We have shown previously  $^{47}$  that the equivalent dielectric constant of a solution of gold core NPs in n-decane oil, which emulates the hydrocarbon interior of the bilayer, reaches an asymptotic minimum value of  $\sim$ 1.8 at frequencies above 10 Hz. The measured value of the dielectric constant for

the NP–oil solution (1.8) is less than 10% higher than what we measured for neat n-decane. Therefore, when membrane capacitance is interrogated using AC voltages at frequencies above 10 Hz, we expect that permittivity would only be marginally higher in the presence of NPs and that the value of permittivity would be a constant. Confirming this, specific capacitance measurements of DIBs containing 15% OT NPs obtained using 10 and 100 Hz AC applied voltages showed statistically similar values of  $C_{\rm m}$  (0.60  $\mu \rm F/cm^2$  for the same bilayer at both frequencies).

Therefore, assuming that the average value of permittivity of the membrane remains constant upon addition of NPs, we calculated the average hydrophobic thickness, d, of the membrane from the measurements of  $C_{\rm m}$ . We assumed a dielectric constant of 2.2 for the hydrophobic interior of the membrane.<sup>47</sup> Figure 6 shows how the calculated value of d

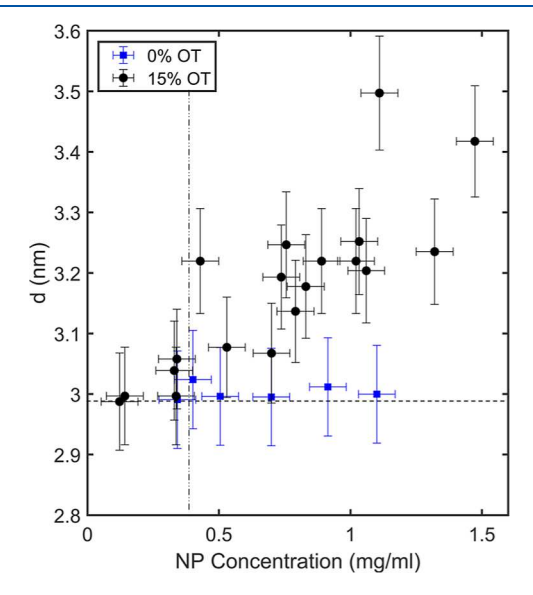


**Figure 6.** Dose-dependent changes of average hydrophobic thickness, d, of DPhPC bilayers after addition of 0% OT or amphiphilic 15% OT NPs at different concentrations. Thickness values are computed from measured  $C_{\rm m}$  values (Figure 2). Thus, the trends versus NP concentration are similar to those for  $C_{\rm m}$ , but inversed. The horizontal dashed line indicates the baseline hydrophobic thickness of a DPhPC bilayer formed in n-hexadecane. The vertical error bars represent the uncertainty in d ( $\pm 0.07$  nm), and horizontal error bars represent the uncertainty in concentration ( $\pm 0.07$  mg/mL).

varies with the NP concentration for 15% OT and 0% OT NPs. The addition of 15% OT NPs, which lowered  $C_{\rm m}$ , resulted in a corresponding increase in average d on the order of 0–0.5 nm. Because no change in  $C_{\rm m}$  was measured for the hydrophilic 0% OT NPs (Figure 2A), the calculated average value of d remains constant at approximately 2.99 nm, matching the reported hydrophobic thickness of a DPhPC DIB in n-hexadecane.  $^{52}$ 

Estimating the Number of NPs in the Membrane. The value of  $C_{\rm m}$  can also be used to estimate the number of NPs present in the bilayer. Discussed in Note S5, this calculation assumes that embedded NPs occupy a projected area within the membrane equal to the square of their solvated diameter (6 nm) and their center of mass are confined to a two-dimensional plane centered between the lipid monolayers. From the NP molecular weight and injected volume, we also calculated the number of injected NPs within the droplet(s)

Table 1. Estimated Number of Membrane-Embedded NPs

PC lipid type	lipid phase	OT ligands (%)	NP conc in cis (mg/mL)	injected NPs (×10 <sup>11</sup> )	$\frac{C_{\rm m}}{(\mu {\rm F/cm^2})}$	d (nm)	embedded NPs (×10 <sup>8</sup> )	NP-occupied area (%)	embedded vs injected NPs (%)
DPh	$H_2O$	n/a	0	0	0.65	2.99	n/a	n/a	n/a
DPh	$H_2O$	0	0.91	2.40	0.65	3.00	<1 <sup>a</sup>	<3.7% <sup>a</sup>	<0.04 <sup>a</sup>
		15	0.74	2.41	0.59	3.30	3.95	12.8	0.16
		15	0.73 <sup>b</sup>	3.27	0.50	3.89	8.03	32.5	0.25
DPh/DO	$H_2O$	15	1.04	2.33	0.52	3.74	4.04	28.2	0.17
	oil	30	0.095	7.49	0.57	3.36	2.85	15.1	0.38
		100 <sup>47</sup>	n/a	n/a	0.24	8.20 <sup>c</sup>	9.42	77.4	n/a

"These upper limit values were calculated using the estimated uncertainty in normalized capacitance. <sup>b</sup>Average concentration of NPs on both sides of the bilayer. <sup>c</sup>The oil used was *n*-decane, which created thicker bilayers even in the absence of NPs. <sup>47</sup>

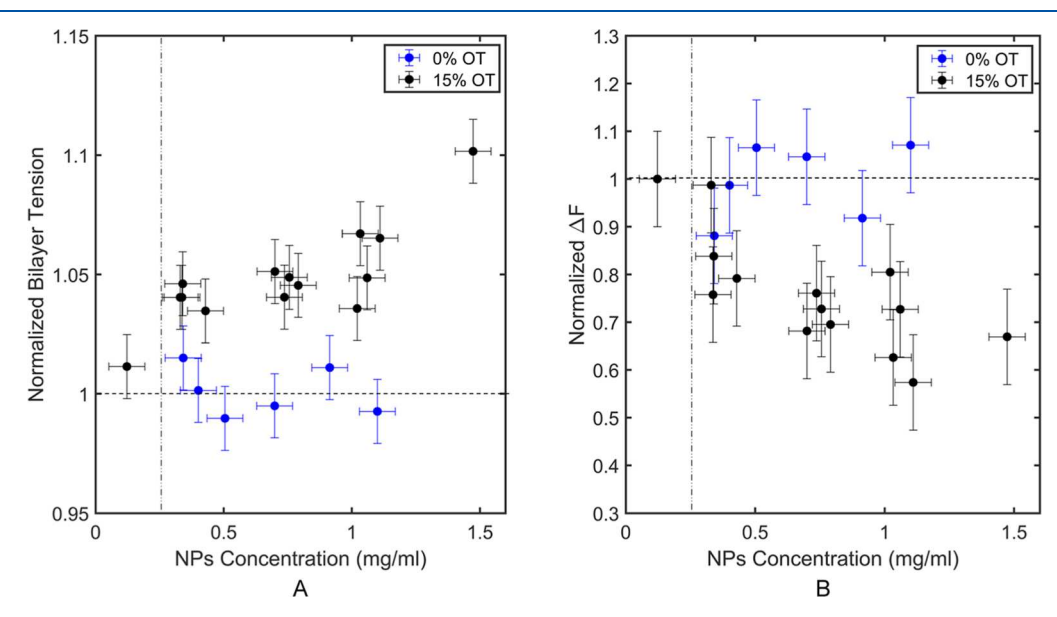


Figure 7. (A) Normalized bilayer tension versus final NP concentration upon the addition of 0% OT or 15% OT NPs into the *cis* droplet of DPhPC DIBs. The vertical error bars represent the uncertainty in normalized bilayer tension ( $\pm 0.013$ ), and the horizontal error bars represent the uncertainty in concentration ( $\pm 0.07$  mg/mL). (B) Normalized changes in bilayer free energy of formation of a DPhPC DIB vs AmNPs concentration in the *cis* droplet of DPhPC DIBs. The vertical error bars represent the uncertainty in normalized  $\Delta F$  ( $\pm 0.1$ ), and the horizontal error bars represent the uncertainty in concentration ( $\pm 0.07$  mg/mL). The horizontal dashed lines in the two graphs indicate the baseline tension and the free energy of formation of a DPhPC DIB formed in *n*-hexadecane in the absence of NPs. The vertical dashed lines denote the minimum concentrations of 15% OT NPs that cause a significant change in each plotted parameter.

and estimated the percentage of injected NPs that interact with the droplet interface bilayer (Table 1). These calculations reveal that approximately 10<sup>8</sup> to 10<sup>9</sup> 15% OT NPs embed into the membrane after direct microinjection into the droplets. This range corresponds to NPs occupying approximately 12-33% of the membrane area, which is significantly lower than the value Basham et al. reported for 100% OT NPs (last row of Table 1) introduced into the DIB via the surrounding oil.<sup>47</sup> The use of *n*-decane as the oil also led to a thicker bilayer that was able to entrap more NPs. 47 Though 0% OT NPs did not significantly affect the capacitance of DPhPC bilayers, which agrees with the results from Carney et al., 68 it is possible that some embed in the membrane, and the measurement sensitivity is not high enough to detect them. Using the estimated uncertainty of 2.64% for normalized specific capacitance, we calculated that NPs would have to occupy at least 3.7% of the bilayer area to detect a significant change in the measured value of specific capacitance. This percentage translates to as many as  $\sim 10^8$  particles in a bilayer with total area  $1.1 \times 10^{-3}$  cm<sup>2</sup>. Prior work has shown clearly that all MUS-coated NPs with core diameters near 2.4 nm can embed within and translocate DOPC bilayers. 41,66 However, it is also

possible that DPhPC lipids, which have branched acyl chains, impede the uptake of 0% OT NPs more than that observed in DOPC bilayers.

AmNPs Increase the Tension and Free Energy of the Bilayer. Monitoring changes in the bilayer tension is a separate way to quantify the interactions between the lipid membrane and NPs. Mechanical equilibrium in a DIB is attained due to a balance of surface tensions, as described by Young's equation<sup>73</sup>

$$\gamma_{\rm b} = 2\gamma_{\rm m} \cos \theta \tag{2}$$

where  $\gamma_b$  is the bilayer tension and  $\gamma_m$  is the monolayer tension at the oil—water interface, which is oriented away from the plane of the bilayer by the contact angle,  $\theta$ . Our previously published results from pendant drop measurements showed that 15% OT NPs do not affect the steady-state monolayer tension,  $\gamma_m$ , of PC lipids at the oil—water interface. Therefore, assuming a monolayer tension value of 1 mN/m, measurements of nominal contact angle obtained from bottom view DIB images were used to calculate the steady-state bilayer tension for varying concentrations of 15% OT NPs added to the *cis* droplet. The dose-dependent reduction in contact angle

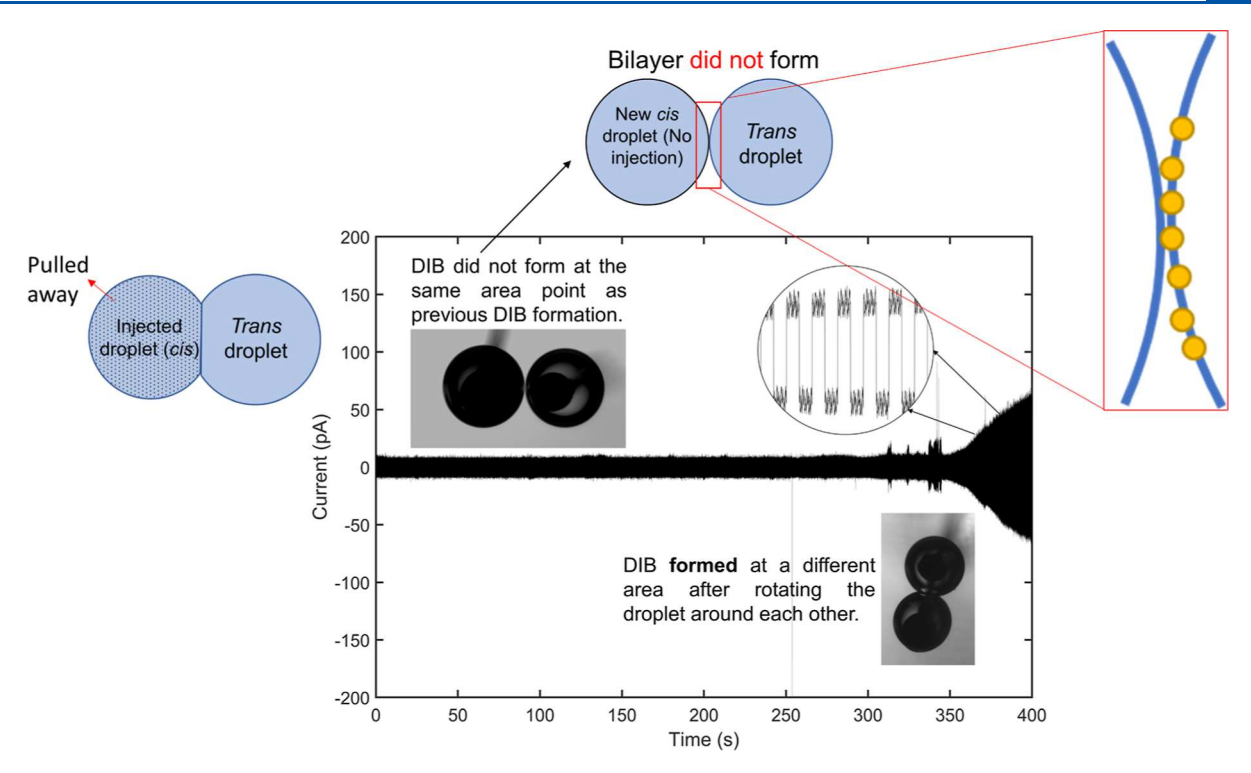


**Figure 8.** Illustration of attempts to form a new bilayer when one of the droplets has been previously exposed to AmNPs. A new bilayer did not form in the precise spot on the *trans* droplet where an NP-affected bilayer had previously formed. In an attempt of forma bilayer on a different section of the *trans* droplet surface, we relocated and rotated it. A new bilayer was formed and reached its maximum capacitance, comparable with the cases with NP injected before bilayer formation.

results in a dose-dependent increase in bilayer tension (Figure 7A). The vertical error bars in this plot represent the uncertainty in measuring the contact angle  $(\pm 1.5^{\circ})$ . Of note, compared to Figure 2A, the threshold for detecting a significant increase in bilayer tension in DPhPC lipid-in DIBs falls to ~0.20 mg/mL. This indicates an increased sensitivity to the effects of embedded NPs by tracking changes in the tension (contact angle). Increases in membrane tension in similar amounts (up to 15%) caused by absorbed NPs have been observed by others as well: hydrophobic or amphiphilic gold NPs stretch or create local curvature in synthetic lipid bilayers<sup>74</sup> and model bacterial bilayers<sup>75</sup> in the amounts close to what we observed (maximum 15%). A change to the contact angle or bilayer tension also implies a change in the free energy of formation,  $\Delta F$ , which quantifies the reduction in free energy of the two-droplet system upon bilayer formation. 73,76,7 Calculated as

$$\Delta F \equiv 2\gamma_{\rm m} - \gamma_{\rm b} = 2\gamma_{\rm m}(1 - \cos \theta) \tag{3}$$

this quantity represents the adhesive strength of the interface and, thus, the amount of energy required per unit area to reversibly separate the opposing monolayer-coated droplets. Figure 7B shows that unlike the 0% OT NPs, the 15% OT NPs injected into the *cis* droplet cause a concentration-dependent reduction in the free energy of formation starting at concentrations slightly below 0.40 mg/mL. The vertical error bars in this plot ( $\pm 0.1$ ) derive from the uncertainty in measuring the contact angle ( $\pm 1.5^{\circ}$ ). The greater bilayer tension (and reduced contact angle) in the presence of sufficient concentrations of AmNPs explains where this reduction originates. Moreover, it shows that the presence of embedded NPs not only changes the lateral force in the membrane but also reduces the normal adhesive force between

droplets that drives the opposing lipid monolayers to exclude excess oil and form a thinned membrane.

Embedded NPs Remain Associated with the Lipids after Droplets Are Separated. Because the two droplets of a DIB can be separated and reconnected after bilayer formation, we were curious about the potential impact of membrane-embedded AmNPs on this process. Therefore, we performed an experiment to separate and reform a new DIB at the same location on one of the two droplets that previously indicated NP uptake (via a reduction in C<sub>m</sub>). Specifically, we removed the original cis droplet and replaced it with a new NPfree lipid-coated droplet that was placed into contact with the original trans droplet. This eliminated the potential of any new NPs to affect the interface and reported instead on the ability of previously embedded NPs to affect the formation of a new membrane. This experiment, including the capacitive current measurement, is shown in Figure 8. Interestingly, when we placed a new droplet in contact with the original trans droplet, a bilayer did not spontaneously form at the same location as the prior DIB even after several minutes. This indicated a barrier existed to spontaneous bilayer thinning. We then revolved the trans droplet a quarter of the way around the new cis droplet at the same z-height to attempt bilayer formation at a different location away from the original location of the NPdoped DIB. At this new point of contact, a bilayer was successfully formed as evidenced by the increase in capacitive current and the right inset image in Figure 8 which shows connected droplets. This difference suggests that NPs embedded in the core of the original DIB remained affiliated with the acyl chains of the lipids coating the trans droplet in sufficient numbers to prevent subsequent bilayer formation with a new cis droplet.

After membrane formation at this new location, the nominal capacitance of the bilayer increased to its maximum value more slowly than the case with no NPs, comparable with the cases with 15% OT NPs before bilayer formation (Supporting Information Note S1). This delayed growth in bilayer capacitance indicates that particles may have diffused along the surface of the lipid monolayer-coated droplet. The presence of NPs on the *trans* interface of the droplet is likely responsible for this phenomenon. Subsequent electrical measurements revealed that this system at the rotated location exhibited the same value of specific capacitance (0.65  $\mu \rm F/cm^2)$  as the bilayer without NPs, demonstrating that the number of affiliated particles was below the minimum threshold for detection. This experiment was performed twice with the same outcome.

#### CONCLUSIONS

Herein, we report on experimentally assessed changes in the specific capacitance and contact angle of droplet interface bilayer model membranes caused by surface-functionalized gold core NPs by leveraging electrophysiological measurements and dual-view imaging. Direct microinjection of stripy amphiphilic NPs into one or both droplets of the DIB after either monolayer preassembly or bilayer formation overcomes the destabilizing effects that these AmNPs exert on bilayer formation. Whereas hydrophilic NPs containing only MUS ligands exhibited no significant effects on DIBs assembled from DPhPC and DOPC lipids, 15% OT and 30% OT striped amphiphilic NPs significantly decreased the steady-state specific capacitance of the bilayer in a concentration-dependent manner for NP concentrations of up to ~1.5 mg/mL (set by the amount of maximum injected volume and the concentration of available NP stock solutions). A net reduction in membrane capacitance matches the findings of previous works<sup>24,46</sup> using different types of amphiphilic functionalized gold NPs. However, unlike prior studies on similar striped AmNPs, we evaluated the area-normalized specific capacitance instead of nominal bilayer capacitance, considered the dielectric permittivity of the particles, and demonstrated that the injection of NPs into both droplets doubled the reduction in  $C_{\rm m}$ . This allowed us to conclude that changes in specific capacitance and contact angle were due to NPs embedding into the hydrophobic core of the membrane, likely at or near the midplane where their hydrophobic OT ligands can maximize favorable interactions with the lipid chains and residual oil. At NP concentrations of 1-1.5 mg/mL, we observed reductions in C<sub>m</sub> on the order of 10-20%, which revealed that embedded NPs cause an estimated increase in the average hydrophobic thickness by as much as 0.5 nm, and they occupy roughly 12-35% of the area of the membrane. The sensitivity of changes in specific capacitance to NP concentrations increased with (1) higher molar fractions of OT on the NP surface, (2) when the lipids were placed in the oil due to the removal of liposomes that offer additional sites for NP-membrane interactions within the droplet, and (3) when unsaturated DOPC lipids were incorporated into the bilayer. Separately, the steady-state contact angle reduced in a concentration-dependent manner upon injection of AmNPs. This finding further revealed that embedded NPs increase the lateral tension of the membrane, a sign that NP inclusions disrupt lipid packing. The measurement sensitivity to changes in lateral tension was slightly better than detecting changes in  $C_{\rm m}$ . Furthermore, our experiments revealed that membraneembedded NPs may remain affiliated with lipid acyl chains even after the two droplets used to form the DIB are physically separated, providing additional proof of their presence in the core of the bilayer.

Through these findings, we showcase the value of using simultaneous electrophysiology and imaging on DIBs to more comprehensively study NP—membrane interactions. Nonetheless, our experiments did not conclusively reveal whether membrane-embedded AmNPs fully translocated the bilayer despite occasional transient changes in membrane conductance. This possibility and the factors that influence it are questions that we continue to investigate. Separately, our recent work on bilayer-entrapped hydrophobic NPs suggests that there are opportunities to study how embedded NPs in the membrane, especially across a wider concentration range, affect the response of the bilayer and also ion channels within it to varying transmembrane voltages.<sup>47</sup>

#### MATERIALS AND METHODS

Materials. Aqueous buffer consists of 1× phosphate-buffered saline (PBS) containing 137 mM NaCl, 2.7 mM KCl, 10 mM Na₂HPO₄, and 1.8 mM KH₂PO₄ buffered with NaOH and HCl to achieve a pH of 7.30 measured via a pH meter (Accumet AP85; Fisher Scientific, USA). Silver wires with 0.125 mm diameter are purchased from Goodfellow Cambridge, Inc. 1,2-diphytanoyl-sn-glycero-3-phosphocholine (DPhPC) and 1,2-dioleoyl-sn-glycero-3-phosphocholine (DOPC) lipids are received as lyophilized powders or dissolved in chloroform from Avanti Polar Lipids, Inc. n-hexadecane oil ( $C_{16}H_{34}$ ) was purchased from Fisher Chemical at ≥98% purity and filtered with Whatman 0.2 μm poly(ether sulfone) membranes prior to use.

NP Preparation. Striped gold NPs with core size distribution centered around 2-3 nm (see the TEM images in Figure S1) and the coatings of either MUS ligands or a combination of MUS and OT ligands were prepared as described elsewhere. <sup>26,43,58,59</sup> All chemicals were purchased from Sigma-Aldrich and used as received. The oleylamine gold NP (OAm-AuNP) 2-3 nm cores were synthesized at 20 °C by dissolving 0.5 mmol of hydrogen tetrachloroaurate(III) trihydrate (HAuCl<sub>4</sub>·3H<sub>2</sub>O, 95%) in a 40 mL solvent mixture of oleylamine (C18 content: 80-90%) and *n*-octane (97%) (1:1 v/v). The solution was sonicated under an argon atmosphere for 10 min before stirring. A 100 mL jacketed flask was used to maintain a temperature of 20 °C. The reducing solution was prepared by dissolving 0.5 mmol of the t-butylamine-borane complex (tBAB, 97%) in 1 mL of oleylamine and 1 mL of octane prior to injection into the precursor solution under vigorous stirring. The mixture was left to react in an argon atmosphere at the specified reaction temperature for 2 h before 30 mL of ethanol was added to quench the reaction. The AuNPs were collected by centrifugation at 500 rpm for 10 min, then redispersed in dichloromethane (DCM), and washed several times with ethanol using centrifugation and redispersion. The powder was dried in a vacuum desiccator. MUS and OT with the appropriate feed ratios were dissolved in DCM: 33% OT and 66% MUS for the 15% OT NPs and 50% OT and 50% MUS for the 30% OT NPs. The ligand mixture solution was added to the NP solution. The reaction was left for 48 h at 350 rpm and room temperature for ligand exchange. The product was then purified using centrifugation and redispersion with ethanol and acetone and finally with water through centrifuge-assisted dialysis using Amicon filtration (MWCO 35 kDa). The filtered material was then dried under a vacuum inside a desiccator before use in experiments. The ratio between MUS and OT was determined using <sup>1</sup>H NMR, following the protocol described elsewhere. 43,78 After rehydrating dry NPs in 1× PBS and 15 min of sonication in a water bath, the colloidal suspensions were extruded 11 times through a Whatman 30 nm polycarbonate membrane in an Avanti Mini Extruder. The 0% OT and 15% OT NPs were prepared at 10 mg/mL and then further diluted to 2 mg/mL. The 30% OT NPs, however, were less soluble in the aqueous phase, and after many hours

of stirring, the maximum achieved concentration was 0.16 mg/mL, determined later via calibration through nanodrop spectrometry provided in the Supporting Information (Note S5).

**Liposome Preparation for Lipid-In DIBs.** Using droplets from aqueous solutions containing large unilamellar vesicles (LUVs), the droplet interface bilayer is formed. Unless otherwise specified, lipids are dissolved to a concentration of 2 mg/mL in an aqueous buffer (1× PBS, pH = 7.30) to produce multilamellar vesicles (MLVs). When lipids with a melting point above room are dissolved temperature, the buffer is initially heated to a temperature higher than the lipid melting point. Fresh MLV solutions are vortexed, aliquoted, and frozen at -20 °C. After five cycles of freezing and thawing, MLV stock solutions are extruded 11 times (Avanti MiniExtruder with Whatman 100 nm polycarbonate filters) to form large unilamellar vesicles (LUV) 100 nm in diameter. Liposomes were stored at 4 °C and usually formed bilayers successfully up to 6 months after preparation.

**Lipid-In-Oil Preparation for Lipid-Out DIBs.** The preparation involves allowing powder lipids that have been dissolved in chloroform to evaporate under a nitrogen stream for 15 min, after which they are left in a desiccator for at least 3 h to ensure complete evaporation of the chloroform. 99% *n*-hexadecane (Thermo Fisher) is added to the dried lipid to yield to a final concentration of 5 mg/mL lipid in oil. The lipid-in-oil sample is then vortexed and sonicated for 30 min before using in the experiment. Lipid-in-oil samples are stored on the shelf at RT and were used within a week from preparation.

**DIB Formation.** DIBs were formed at RT (22 °C) between two aqueous droplets of LUV solution (or droplets of 1× PBS when lipid is dissolved in oil) suspended on agarose-coated silver-silver chloride wire-type electrodes in a square-shaped glass cuvette to accommodate both bottom and side views, as described elsewhere. 51 Aqueous droplets (between 150 and 300 nL in volume depending on target NP concentration) of 1× PBS containing 2 mg/mL lipid vesicles were deposited onto Ag/AgCl electrodes connected to an Axopatch 200B patch clamp amplifier, which supplied DC voltage and measured current. The controlled head stage voltage was supplied to the electrode in the trans droplet, while the electrode in the cis droplet was connected to ground. All measurements were performed with proper shielding to limit background noise, and the induced current signal was digitized by using a Digidata 1440 data acquisition device (Molecular Devices). The measured current induced by a 10 Hz, 10 mV triangle voltage waveform output from a function generator (Agilent) is used to determine nominal bilayer capacitance. The dimensions of the oval-shaped contact area (vertical dimension acquired from the side view and horizontal from the bottom view) are used to calculate the bilayer area using a custom image processing script in MATLAB. The specific membrane capacitance  $(C_{\rm m})$  is calculated from linear regression of bilayer capacitance and bilayer area data measured simultaneously for different levels of contact between droplets achieved by varying the horizontal distance between electrodes.

Capillary Pulling for Microinjection of NPs. Pulled glass capillaries (microtips) were used to inject AmNPs into the droplets. Injection micropipettes were made from borosilicate capillaries (1 mm o.d., 0.58 mm i.d., GC100-15; Fisher Scientific) using a laser-heated pipet puller (P-2000; Sutter). Even though the instrument has two default settings for borosilicate glasses, both of them made microtips with openings that were either too large (tens of  $\mu$ m) which caused bilayer failure during injection or too narrow (below 200 nm) which were more likely to get blocked. We were able to make microtips with the proper opening diameter (1.5  $\mu$ m) for this system by changing the pulling parameters. Specifically, we changed the pulling force, the pulling velocity (the speed at which the puller bar must be moving before the final hard pull is executed), and the delay parameter, which controls when the hard pull begins in relation to when the laser is turned off.

**NP Microinjection Technique.** A flexible needle microloader (MF34G-5; World Precision Instruments) mounted on a glass syringe was used to load the pulled microtips with an aqueous solution containing AmNPs. The loaded microtip was then mounted on a motorized micromanipulator (MM-92VR; Narishige International

USA, Inc.) as shown in Figure S3. The aqueous NP solution was dispensed by controlling the internal pressure of the microtip by using a pneumatic injector (IM-11-2; Narishige International USA, Inc.). The amount of NP solution injected is governed by the amount and duration of applied pressure and the diameter of the microtip. Due to variations in the position and shape of the air—solution meniscus within the microtip, the pressure at the opening of the microtip may vary by hundreds of pascals. We manually varied the applied pressure to the injector to compensate for this intrinsic offset: pressure was adjusted to stably advance the solution to the end of the pipet tip. After this zero-pressure point was established, the microtip was slowly inserted into the cis droplet. Pressure was then increased once more to establish an outward flow of NP solution.

Determination of Final NP Concentration in the Droplet. To calculate the final concentration of NPs in the injected droplet, a geometrical approach was employed to determine the final volume of the injected droplet (Note S2). We used the injected droplet's dimensions acquired from two angles to estimate its volume before and after the injection and used the added NP solution's volume and initial concentration to estimate the final NP concentration in the droplet. Since the hanging droplet is more egg-shaped than ovoid-shaped, there will be some estimation error, but comparing the calculated volume with the volume change in initial NP solution in the microtip, the difference for injected volume was below 3% in multiple trials. The droplets' pre- and postinjection volume is used for calculations for the reported data in this paper.

The final NP concentration  $C_f$  is calculated as follow

$$C_{\rm f} = \frac{C_0 \nu_0 + C_{\rm utip}(\nu_{\rm f} - \nu_0)}{\nu_{\rm f}} \tag{4}$$

where  $C_0$  is the initial NP concentration (equal to zero before the first injection),  $C_{\text{utip}}$  is the NP concentration in the microtip, and  $\nu_0$  and  $\nu_f$  are initial and final volume of the cis droplet, respectively.

Uncertainty Analysis and Statistics. The two methods used to estimate injected volume differed by approximately 5% in value, which translates into an uncertainty of  $\pm 0.07$  mg/mL difference for the maximum NP concentration tested (1.4 mg/mL). For lipid-out experiments and results shown in Figure 3, where the maximum NP concentration is 0.16 mg/mL, the uncertainty was  $\pm 0.02$  mg/mL.

The acquired  $C_{\rm m}$  values were sensitive to error stemming from both current and area measurements due to electrical noise and uncertainty in image acquisition, respectively. As electrical noise was considerably diminished in our system,  $C_{\rm m}$  values were deemed most sensitive to measurements of the bilayer major axis since the pixels were largest in the side-view camera. Thus, to consider the effect of error in area calculations on the sensitivity of our system, the uncertainty in the projected length of the bilayer was assumed to be about  $\pm 5$  pixels ( $\pm 20~\mu{\rm m}$ ) along the major axis. This uncertainty results in  $\pm 2.64\%$  uncertainty in the value of  $C_{\rm m}$ . These are reflected as error bars in Figures 2, 3, 4, and 6. The corresponding uncertainty in the hydrophobic thickness is estimated to be  $\pm 0.07$  nm.

The uncertainty for contact angle measurements (Figure 2B) is calculated as the highest standard deviation among multiple preinjection experiments equal to  $\pm 1.5^{\circ}$ . Using eqs 2 and 3, this result is utilized to compute an uncertainty of for normalized bilayer tension and  $\pm 0.1$  for normalized changes in bilayer free energy (Figure 7).

To estimate the minimum threshold of NP concentration required to induce a statistically significant change in a measured quantity (e.g.,  $C_{\rm m}$ ,  $\theta$ , etc.), we employed an iterative procedure in which a candidate concentration threshold was selected to create two subsets of the data at lower and higher concentrations, sets 1 and 2, respectively. Each of these subsets was compared using a two-tailed student *t*-test (assuming unequal variances) to the average response measured for the baseline case in the absence of NPs. If both set 1 and set 2 were statistically different ( $p \geq 0.05$ ), then the threshold position was lowered, and the process was repeated on the newly divided subsets of the data until only set 1 was statistically similar and set 2 was statistically different. The minimum concentration at which these

conditions were met was adopted as the minimum threshold, shown as a vertical dashed line on the plots.

#### ASSOCIATED CONTENT

#### **Solution** Supporting Information

The Supporting Information is available free of charge at https://pubs.acs.org/doi/10.1021/acs.langmuir.3c01973.

Electromicrographs of NPs; schematic of the DIB microinjection setup; prebilayer injection delays bilayer formation; AmNPs can cause leakage current; calculating the final concentration of NPs in the microinjected droplet; changes in contact angle and the position of the cis droplet immediately after until 30 min after the injection; fitting the concentration of 15% with absorbance at 550 nm to estimate the final concentration of 30% OT samples after dissolving in aqueous buffer; electrowetting experiment to measure the dipole potential of the membrane in the presence of 15% OT NP on one side of the bilayer; estimating the number of NPs in the bilayer from thickness measurements; and references (PDF)

Buffer injection (MOV)

#### AUTHOR INFORMATION

#### **Corresponding Author**

Stephen A. Sarles — Department of Mechanical, Aerospace and Biomedical Engineering, University of Tennessee, Knoxville, Tennessee 37996, United States; orcid.org/0000-0002-6694-6451; Email: ssarles@utk.edu

#### **Authors**

Farzin Mashali — Department of Mechanical, Aerospace and Biomedical Engineering, University of Tennessee, Knoxville, Tennessee 37996, United States; ⊚ orcid.org/0000-0002-5178-674X

Colin M. Basham — Department of Mechanical, Aerospace and Biomedical Engineering, University of Tennessee, Knoxville, Tennessee 37996, United States; orcid.org/0000-0002-4364-221X

Xufeng Xu – Institute of Materials, École Polytechnique Fédérale de Lausanne (EPFL), Lausanne CH-1015, Switzerland

Camilla Servidio — Institute of Materials, École Polytechnique Fédérale de Lausanne (EPFL), Lausanne CH-1015, Switzerland

Paulo H. Jacob Silva – Institute of Materials, École Polytechnique Fédérale de Lausanne (EPFL), Lausanne CH-1015, Switzerland

Francesco Stellacci — Institute of Materials, École Polytechnique Fédérale de Lausanne (EPFL), Lausanne CH-1015, Switzerland

Complete contact information is available at: https://pubs.acs.org/10.1021/acs.langmuir.3c01973

#### **Author Contributions**

F.M. and C.B. performed all experiments. X.X., C.S., and P.H.J.S. synthesized and characterized NPs. F.M., C.B., and S.A.S. devised the experiments. All authors contributed to the writing and editing of the manuscript. F.S. and S.A.S. provided financial support for the work.

#### Notes

The authors declare no competing financial interest.

#### ACKNOWLEDGMENTS

F.M., C.B., and S.A.S. acknowledge the financial support from the National Science Foundation through CAREER Grant CBET-1752197. S.A.S. acknowledges the financial support from the James Conklin Faculty Fellowship at the University of Tennessee, Knoxville. The authors would like to acknowledge Dr. Bhavya Sharma and Avery Woods for use of the micropipette puller instrument and Dr. Scott Lenaghan for use of the NanoDrop Microvolume spectrophotometer.

#### REFERENCES

(1) Gautam, A.; van Veggel, F. C. J. M. Synthesis of Nanoparticles, Their Biocompatibility, and Toxicity Behavior for Biomedical Applications. *J. Mater. Chem. B* **2013**, *1* (39), 5186–5200.

(2) Paris, J. L.; Baeza, A.; Vallet-Regí, M. Overcoming the Stability, Toxicity, and Biodegradation Challenges of Tumor Stimuli-Responsive Inorganic Nanoparticles for Delivery of Cancer Therapeutics. *Expert Opin. Drug Delivery* **2019**, *16* (10), 1095–1112.

(3) Zor, F.; Selek, F. N.; Orlando, G.; Williams, D. F. Biocompatibility in Regenerative Nanomedicine. *Nanomedicine* **2019**, *14* (20), 2763–2775.

(4) Nikzamir, M.; Akbarzadeh, A.; Panahi, Y. An Overview on Nanoparticles Used in Biomedicine and Their Cytotoxicity. *J. Drug Delivery Sci. Technol.* **2021**, *61*, 102316.

(5) Wang, Y.; Cai, R.; Chen, C. The Nano-Bio Interactions of Nanomedicines: Understanding the Biochemical Driving Forces and Redox Reactions. *Acc. Chem. Res.* **2019**, 52 (6), 1507–1518.

(6) Cai, X.; Liu, X.; Jiang, J.; Gao, M.; Wang, W.; Zheng, H.; Xu, S.; Li, R. Molecular Mechanisms, Characterization Methods, and Utilities of Nanoparticle Biotransformation in Nanosafety Assessments. *Small* **2020**, *16* (36), 1907663.

(7) Contini, C.; Schneemilch, M.; Gaisford, S.; Quirke, N. Nanoparticle-Membrane Interactions. *J. Exp. Nanosci.* **2018**, *13* (1), 62–81.

(8) Mitchell, M. J.; Billingsley, M. M.; Haley, R. M.; Wechsler, M. E.; Peppas, N. A.; Langer, R. Engineering Precision Nanoparticles for Drug Delivery. *Nat. Rev. Drug Discovery* **2021**, *20* (2), 101–124.

(9) Lee, S. W.; Park, S. D.; Kang, S.; Bang, I. C.; Kim, J. H. Investigation of Viscosity and Thermal Conductivity of SiC Nanofluids for Heat Transfer Applications. *Int. J. Heat Mass Transfer* **2011**, *54* (1–3), 433–438.

(10) Sardoiwala, M. N.; Kaundal, B.; Roy Choudhury, S. Development of Engineered Nanoparticles Expediting Diagnostic and Therapeutic Applications across Blood-Brain Barrier. In *Handbook of Nanomaterials for Industrial Applications*; Elsevier, 2018; pp 696–709.

(11) Rai, P.; Mallidi, S.; Zheng, X.; Rahmanzadeh, R.; Mir, Y.; Elrington, S.; Khurshid, A.; Hasan, T. Development and Applications of Photo-Triggered Theranostic Agents. *Adv. Drug Delivery Rev.* **2010**, 62 (11), 1094–1124.

(12) Biswas, A.; Shukla, A.; Maiti, P. Biomaterials for Interfacing Cell Imaging and Drug Delivery: An Overview. *Langmuir* **2019**, 35 (38), 12285–12305.

(13) Witwer, K. W.; Wolfram, J. Extracellular Vesicles versus Synthetic Nanoparticles for Drug Delivery. *Nat. Rev. Mater.* **2021**, 6 (2), 103–106.

(14) Jamburidze, A.; Huerre, A.; Baresch, D.; Poulichet, V.; De Corato, M.; Garbin, V. Nanoparticle-Coated Microbubbles for Combined Ultrasound Imaging and Drug Delivery. *Langmuir* **2019**, 35 (31), 10087–10096.

(15) Ali Dheyab, M.; Abdul Aziz, A.; Jameel, M. S.; Moradi Khaniabadi, P.; Oglat, A. A. Rapid Sonochemically-Assisted Synthesis of Highly Stable Gold Nanoparticles as Computed Tomography Contrast Agents. *Appl. Sci.* **2020**, *10* (20), 7020.

(16) Elahi, N.; Kamali, M.; Baghersad, M. H. Recent Biomedical Applications of Gold Nanoparticles: A Review. *Talanta* **2018**, *184*, 537–556.

- (17) Kus-Liśkiewicz, M.; Fickers, P.; Ben Tahar, I. Biocompatibility and Cytotoxicity of Gold Nanoparticles: Recent Advances in Methodologies and Regulations. *Int. J. Mol. Sci.* **2021**, 22 (20), 10952.
- (18) Lin, J.; Zhang, H.; Chen, Z.; Zheng, Y. Penetration of Lipid Membranes by Gold Nanoparticles: Insights into Cellular Uptake, Cytotoxicity, and Their Relationship. *ACS Nano* **2010**, *4* (9), 5421–5429.
- (19) Zeng, S.; Yong, K.-T.; Roy, I.; Dinh, X.-Q.; Yu, X.; Luan, F. A Review on Functionalized Gold Nanoparticles for Biosensing Applications. *Plasmonics* **2011**, *6*, 491–506.
- (20) Cardellini, J.; Caselli, L.; Lavagna, E.; Salassi, S.; Amenitsch, H.; Calamai, M.; Montis, C.; Rossi, G.; Berti, D. Membrane Phase Drives the Assembly of Gold Nanoparticles on Biomimetic Lipid Bilayers. *J. Phys. Chem. C* **2022**, *126* (9), 4483–4494.
- (21) Salassi, S.; Caselli, L.; Cardellini, J.; Lavagna, E.; Montis, C.; Berti, D.; Rossi, G. A Martini Coarse Grained Model of Citrate-Capped Gold Nanoparticles Interacting with Lipid Bilayers. *J. Chem. Theory Comput.* **2021**, *17* (10), 6597–6609.
- (22) Contini, C.; Hindley, J. W.; Macdonald, T. J.; Barritt, J. D.; Ces, O.; Quirke, N.-C. Size Dependency of Gold Nanoparticles Interacting with Model Membranes. *Commun. Chem.* **2020**, *3*, 130.
- (23) Kariuki, R.; Penman, R.; Bryant, S. J.; Orrell-Trigg, R.; Meftahi, N.; Crawford, R. J.; McConville, C. F.; Bryant, G.; Voitchovsky, K.; Conn, C. E.; et al. Behavior of Citrate-Capped Ultrasmall Gold Nanoparticles on a Supported Lipid Bilayer Interface at Atomic Resolution. ACS Nano 2022, 16 (10), 17179–17196.
- (24) Guo, Y.; Terazzi, E.; Seemann, R.; Fleury, J. B.; Baulin, V. A. Direct Proof of Spontaneous Translocation of Lipid-Covered Hydrophobic Nanoparticles through a Phospholipid Bilayer. *Sci. Adv.* **2016**, 2 (11), No. e1600261.
- (25) Quan, X.; Peng, C.; Zhao, D.; Li, L.; Fan, J.; Zhou, J. Molecular Understanding of the Penetration of Functionalized Gold Nanoparticles into Asymmetric Membranes. *Langmuir* **2017**, 33 (1), 361–371.
- (26) Verma, A.; Uzun, O.; Hu, Y.; Hu, Y.; Han, H.-S.; Watson, N.; Chen, S.; Irvine, D. J.; Stellacci, F. Surface-Structure-Regulated Cell-Membrane Penetration by Monolayer-Protected Nanoparticles. *Nat. Mater.* **2008**, *7* (7), 588–595.
- (27) Verma, A.; Stellacci, F. Effect of Surface Properties on Nanoparticle-Cell Interactions. *Small* **2010**, *6* (1), 12–21.
- (28) Chu, Z.; Zhang, S.; Zhang, B.; Zhang, C.; Fang, C.-Y.; Rehor, I.; Cigler, P.; Chang, H.-C.; Lin, G.; Liu, R.; et al. Unambiguous Observation of Shape Effects on Cellular Fate of Nanoparticles. *Sci. Rep.* **2014**, *4* (1), 4495.
- (29) Yang, S.; Liu, Y.; Wang, Y.; Cao, A. Biosafety and Bioapplication of Nanomaterials by Designing Protein-Nanoparticle Interactions. *Small* **2013**, *9* (9–10), 1635–1653.
- (30) Buchman, J. T.; Hudson-Smith, N. V.; Landy, K. M.; Haynes, C. L. Understanding Nanoparticle Toxicity Mechanisms to Inform Redesign Strategies to Reduce Environmental Impact. *Acc. Chem. Res.* **2019**, 52 (6), 1632–1642.
- (31) Lalatsa, A.; Schätzlein, A. G.; Mazza, M.; Le, T. B. H.; Uchegbu, I. F. Amphiphilic Poly (l-Amino Acids)—New Materials for Drug Delivery. *J. Controlled Release* **2012**, *161* (2), 523–536.
- (32) Kuna, J. J.; Voïtchovsky, K.; Singh, C.; Jiang, H.; Mwenifumbo, S.; Ghorai, P. K.; Stevens, M. M.; Glotzer, S. C.; Stellacci, F. The Effect of Nanometre-Scale Structure on Interfacial Energy. *Nat. Mater.* **2009**, *8* (10), 837–842.
- (33) Yang, Y.-S.; Carney, R. P.; Stellacci, F.; Irvine, D. J. Enhancing Radiotherapy by Lipid Nanocapsule-Mediated Delivery of Amphiphilic Gold Nanoparticles to Intracellular Membranes. *ACS Nano* **2014**, *8* (9), 8992–9002.
- (34) Jewell, C. M.; Jung, J.; Atukorale, P. U.; Carney, R. P.; Stellacci, F.; Irvine, D. J. Oligonucleotide Delivery by Cell-Penetrating "Striped" Nanoparticles. *Angew. Chem.* **2011**, *123* (51), 12520–12523.
- (35) Luo, Z.; Marson, D.; Ong, Q. K.; Loiudice, A.; Kohlbrecher, J.; Radulescu, A.; Krause-Heuer, A.; Darwish, T.; Balog, S.; Buonsanti, R.; et al. Quantitative 3D Determination of Self-Assembled Structures

- on Nanoparticles Using Small Angle Neutron Scattering. Nat. Commun. 2018, 9 (1), 1343.
- (36) Luo, Z.; Zhao, Y.; Darwish, T.; Wang, Y.; Hou, J.; Stellacci, F. Mass Spectrometry and Monte Carlo Method Mapping of Nanoparticle Ligand Shell Morphology. *Nat. Commun.* **2018**, 9 (1), 4478.
- (37) Van Lehn, R. C.; Alexander-Katz, A. Energy Landscape for the Insertion of Amphiphilic Nanoparticles into Lipid Membranes: A Computational Study. *PLoS One* **2019**, *14* (1), No. e0209492.
- (38) Carney, R. P.; DeVries, G. A.; Dubois, C.; Kim, H.; Kim, J. Y.; Singh, C.; Ghorai, P. K.; Tracy, J. B.; Stiles, R. L.; Murray, R. W.; et al. Size Limitations for the Formation of Ordered Striped Nanoparticles. *J. Am. Chem. Soc.* **2008**, *130* (3), 798–799.
- (39) Yang, Y.-S. S.; Atukorale, P. U.; Moynihan, K. D.; Bekdemir, A.; Rakhra, K.; Tang, L.; Stellacci, F.; Irvine, D. J. High-Throughput Quantitation of Inorganic Nanoparticle Biodistribution at the Single-Cell Level Using Mass Cytometry. *Nat. Commun.* **2017**, *8* (1), 14069.
- (40) Canepa, E.; Salassi, S.; de Marco, A. L.; Lambruschini, C.; Odino, D.; Bochicchio, D.; Canepa, F.; Canale, C.; Dante, S.; Brescia, R.; et al. Amphiphilic Gold Nanoparticles Perturb Phase Separation in Multidomain Lipid Membranes. *Nanoscale* **2020**, *12* (38), 19746–19759
- (41) Van Lehn, R. C.; Atukorale, P. U.; Carney, R. P.; Yang, Y.-S.; Stellacci, F.; Irvine, D. J.; Alexander-Katz, A. Effect of Particle Diameter and Surface Composition on the Spontaneous Fusion of Monolayer-Protected Gold Nanoparticles with Lipid Bilayers. *Nano Lett.* 2013, 13 (9), 4060–4067.
- (42) Carney, R. P.; Astier, Y.; Carney, T. M.; Voïtchovsky, K.; Jacob Silva, P. H.; Stellacci, F.; Al, C. E. T. Electrical Method to Quantify Nanoparticle Interaction with Lipid Bilayers. *ACS Nano* **2013**, 7 (2), 932–942.
- (43) Van Lehn, R. C.; Ricci, M.; Silva, P. H. J.; Andreozzi, P.; Reguera, J.; Voïtchovsky, K.; Stellacci, F.; Alexander-Katz, A. Lipid Tail Protrusions Mediate the Insertion of Nanoparticles into Model Cell Membranes. *Nat. Commun.* **2014**, *5*, 4482.
- (44) Najem, J. S.; Hasan, M. S.; Williams, R. S.; Weiss, R. J.; Rose, G. S.; Taylor, G. J.; Sarles, S. A.; Collier, C. P. Dynamical Nonlinear Memory Capacitance in Biomimetic Membranes. *Nat. Commun.* **2019**, *10* (1), 3239.
- (45) Taylor, G.; Nguyen, M.-A.; Koner, S.; Freeman, E.; Collier, C. P.; Sarles, S. A. Electrophysiological Interrogation of Asymmetric Droplet Interface Bilayers Reveals Surface-Bound Alamethicin Induces Lipid Flip-Flop. *Biochim. Biophys. Acta, Biomembr.* **2019**, 1861 (1), 335–343.
- (46) Fleury, J.-B.; Werner, M.; Guével, X. L.; Baulin, V. A. Protein Corona Modulates Interaction of Spiky Nanoparticles with Lipid Bilayers. *J. Colloid Interface Sci.* **2021**, *603*, 550–558.
- (47) Basham, C. M.; Spittle, S.; Sangoro, J.; El-Beyrouthy, J.; Freeman, E.; Sarles, S. A. Entrapment and Voltage-Driven Reorganization of Hydrophobic Nanoparticles in Planar Phospholipid Bilayers. ACS Appl. Mater. Interfaces 2022, 14 (49), 54558–54571.
- (48) Bayley, H.; Cronin, B.; Heron, A.; Holden, M. A.; Hwang, W. L.; Syeda, R.; Thompson, J.; Wallace, M. Droplet Interface Bilayers. *Mol. BioSyst.* **2008**, *4* (12), 1191–1208.
- (49) Gross, L. C. M.; Heron, A. J.; Baca, S. C.; Wallace, M. I. Determining Membrane Capacitance by Dynamic Control of Droplet Interface Bilayer Area. *Langmuir* **2011**, *27* (23), 14335–14342.
- (50) El-Beyrouthy, J.; Makhoul-Mansour, M. M.; Taylor, G.; Sarles, S. A.; Freeman, E. C. A New Approach for Investigating the Response of Lipid Membranes to Electrocompression by Coupling Droplet Mechanics and Membrane Biophysics. *J. R. Soc., Interface* **2019**, *16* (161), 20190652.
- (51) Taylor, G. J.; Sarles, S. A. Heating-Enabled Formation of Droplet Interface Bilayers Using Escherichia Coli Total Lipid Extract. *Langmuir* **2015**, *31*, 325–337.
- (52) Taylor, G. J.; Venkatesan, G. A.; Collier, C. P.; Sarles, S. A. Direct in Situ Measurement of Specific Capacitance, Monolayer Tension, and Bilayer Tension in a Droplet Interface Bilayer. *Soft Matter* **2015**, *11* (38), 7592–7605.

- (53) Koner, S.; Tawfik, J.; Mashali, F.; Kennison, K. B.; McClintic, W. T.; Heberle, F. A.; Tu, Y.-M.; Kumar, M.; Sarles, S. A. Homogeneous Hybrid Droplet Interface Bilayers Assembled from Binary Mixtures of DPhPC Phospholipids and PB-b-PEO Diblock Copolymers. *Biochim. Biophys. Acta, Biomembr.* **2022**, *1864* (10), 183997.
- (54) Basham, C. M.; Premadasa, U. I.; Ma, Y.-Z.; Stellacci, F.; Doughty, B.; Sarles, S. A. Nanoparticle-Induced Disorder at Complex Liquid-Liquid Interfaces: Effects of Curvature and Compositional Synergy on Functional Surfaces. *ACS Nano* **2021**, *15* (9), 14285–14294.
- (55) Allen-Benton, M.; Findlay, H. E.; Booth, P. J. Probing Membrane Protein Properties Using Droplet Interface Bilayers. *Exp. Biol. Med.* **2019**, 244 (8), 709–720.
- (56) Rojko, N.; Cronin, B.; Danial, J. S. H.; Baker, M. A. B.; Anderluh, G.; Wallace, M. I. Imaging the Lipid-Phase-Dependent Pore Formation of Equinatoxin II in Droplet Interface Bilayers. *Biophys. J.* **2014**, *106* (8), 1630–1637.
- (57) Booth, M. J.; Restrepo Schild, V.; Downs, F. G.; Bayley, H. Functional Aqueous Droplet Networks. *Mol. BioSyst.* **2017**, *13* (9), 1658–1691.
- (58) Guven, Z. P.; Silva, P. H. J.; Luo, Z.; Cendrowska, U. B.; Gasbarri, M.; Jones, S. T.; Stellacci, F. Synthesis and Characterization of Amphiphilic Gold Nanoparticles. *J. Visualized Exp.* **2019**, No. 149, No. e58872.
- (59) Yang, Y.; Serrano, L. A.; Guldin, S. A Versatile AuNP Synthetic Platform for Decoupled Control of Size and Surface Composition. *Langmuir* **2018**, *34* (23), 6820–6826.
- (60) Venkatesan, G. A.; Lee, J.; Farimani, A. B.; Heiranian, M.; Collier, C. P.; Aluru, N. R.; Sarles, S. A. Adsorption Kinetics Dictate Monolayer Self-Assembly for Both Lipid-in and Lipid-out Approaches to Droplet Interface Bilayer Formation. *Langmuir* **2015**, *31* (47), 12883–12893.
- (61) Huang, Y.; Fuller, G. G.; Chandran Suja, V. Physicochemical Characteristics of Droplet Interface Bilayers. *Adv. Colloid Interface Sci.* **2022**, *304*, 102666.
- (62) Pan, J.; Tristram-Nagle, S.; Kučerka, N.; Nagle, J. F. Temperature Dependence of Structure, Bending Rigidity, and Bilayer Interactions of Dioleoylphosphatidylcholine Bilayers. *Biophys. J.* **2008**, 94 (1), 117–124.
- (63) Zakharova, A. A.; Efimova, S. S.; Malev, V. V.; Ostroumova, O. S. Fengycin Induces Ion Channels in Lipid Bilayers Mimicking Target Fungal Cell Membranes. *Sci. Rep.* **2019**, *9* (1), 16034.
- (64) Venkatesan, G. A.; Taylor, G. J.; Basham, C. M.; Brady, N. G.; Collier, C. P.; Sarles, S. A. Evaporation-Induced Monolayer Compression Improves Droplet Interface Bilayer Formation Using Unsaturated Lipids. *Biomicrofluidics* **2018**, *12* (2), 24101.
- (65) Goreham, R. V.; Thompson, V. C.; Samura, Y.; Gibson, C. T.; Shapter, J. G.; Köper, I. Interaction of Silver Nanoparticles with Tethered Bilayer Lipid Membranes. *Langmuir* **2015**, *31* (21), 5868–5874
- (66) Atukorale, P. U.; Guven, Z. P.; Bekdemir, A.; Carney, R. P.; Van Lehn, R. C.; Yun, D. S.; Jacob Silva, P. H.; Demurtas, D.; Yang, Y.-S.; Alexander-Katz, A.; et al. Structure-Property Relationships of Amphiphilic Nanoparticles That Penetrate or Fuse Lipid Membranes. *Bioconjugate Chem.* **2018**, *29* (4), 1131–1140.
- (67) Taylor, G. J.; Heberle, F. A.; Seinfeld, J. S.; Katsaras, J.; Collier, C. P.; Sarles, S. A. Capacitive Detection of Low-Enthalpy, Higher-Order Phase Transitions in Synthetic and Natural Composition Lipid Membranes. *Langmuir* **2017**, 33 (38), 10016–10026.
- (68) Carney, R. P.; Astier, Y.; Carney, T. M.; Voïtchovsky, K.; Jacob Silva, P. H.; Stellacci, F.; Al, C. E. T. Electrical Method to Quantify Nanoparticle Interaction with Lipid Bilayers. *ACS Nano* **2013**, *7* (2), 932–942.
- (69) Dimova, R. Recent Developments in the Field of Bending Rigidity Measurements on Membranes. *Adv. Colloid Interface Sci.* **2014**, 208, 225–234.
- (70) Carney, R. P.; Astier, Y.; Carney, T. M.; Voïtchovsky, K.; Jacob Silva, P. H.; Stellacci, F.; Al, C. E. T. Electrical Method to Quantify

- Nanoparticle Interaction with Lipid Bilayers. ACS Nano 2013, 7 (2), 932–942.
- (71) Sodt, A. J.; Pastor, R. W. Bending Free Energy from Simulation: Correspondence of Planar and Inverse Hexagonal Lipid Phases. *Biophys. J.* **2013**, *104* (10), 2202–2211.
- (72) Abdelhalim, M. A. K.; Mady, M. M.; Ghannam, M. M. Rheological and Dielectric Properties of Different Gold Nanoparticle Sizes. *Lipids Health Dis.* **2011**, *10* (1), 208.
- (73) Needham, D.; Haydon, D. A. Tensions and Free Energies of Formation of "Solventless" Lipid Bilayers. Measurement of High Contact Angles. *Biophys. J.* **1983**, *41* (3), 251–257.
- (74) Li, S.; Malmstadt, N. Deformation and Poration of Lipid Bilayer Membranes by Cationic Nanoparticles. *Soft Matter* **2013**, 9 (20), 4969–4976.
- (75) Linklater, D. P.; Baulin, V. A.; Le Guével, X.; Fleury, J.; Hanssen, E.; Nguyen, T. H. P.; Juodkazis, S.; Bryant, G.; Crawford, R. J.; Stoodley, P. Antibacterial Action of Nanoparticles by Lethal Stretching of Bacterial Cell Membranes. *Adv. Mater.* **2020**, *32* (52), 2005679.
- (76) Thiam, A. R.; Bremond, N.; Bibette, J. From Stability to Permeability of Adhesive Emulsion Bilayers. *Langmuir* **2012**, 28 (15), 6291–6298.
- (77) Dixit, S. S.; Pincus, A.; Guo, B.; Faris, G. W. Droplet Shape Analysis and Permeability Studies in Droplet Lipid Bilayers. *Langmuir* **2012**, 28 (19), 7442–7451.
- (78) Guven, Z. P.; Silva, P. H. J.; Luo, Z.; Cendrowska, U. B.; Gasbarri, M.; Jones, S. T.; Stellacci, F. Synthesis and Characterization of Amphiphilic Gold Nanoparticles. *J. Visualized Exp.* **2019**, No. 149, No. e58872.
- (79) Garten, M.; Mosgaard, L. D.; Bornschlögl, T.; Dieudonné, S.; Bassereau, P.; Toombes, G. E. S. Whole-GUV Patch-Clamping. *Proc. Natl. Acad. Sci. U.S.A.* **2017**, *114* (2), 328–333.

### **□** Recommended by ACS

PRODAN Photophysics as a Tool to Determine the Bilayer Properties of Different Unilamellar Vesicles Composed of Phospholipids

María. A. Luna, N. Mariano Correa, et al.

DECEMBER 15, 2023

LANGMUIR

READ 🗹

Modulation of Phase Behavior and Microscopic Dynamics in Cationic Vesicles by 1-Decyl-3-methylimidazolium Bromide

Jyoti Gupta, Subhankur Mitra, et al.

DECEMBER 21, 2023

LANGMUIR

READ 🗹

Cryo-TEM Reveals the Influence of Multivalent Charge and PEGylation on Shape Transitions in Fluid Lipid Assemblies: From Vesicles to Discs, Rods, and Spheres

Victoria M. Steffes, Cyrus R. Safinya, et al.

DECEMBER 05, 2023

LANGMUIR

READ **C** 

## **Charged Lipids Modulate the Phase Separation in Multicomponent Membranes**

Yifei Wang and Sheereen Majd

JULY 24, 2023

LANGMUIR

READ 🗹

Get More Suggestions >